Molecular Cell

Article

NRF1 association with AUTS2-Polycomb mediates specific gene activation in the brain

Graphical abstract

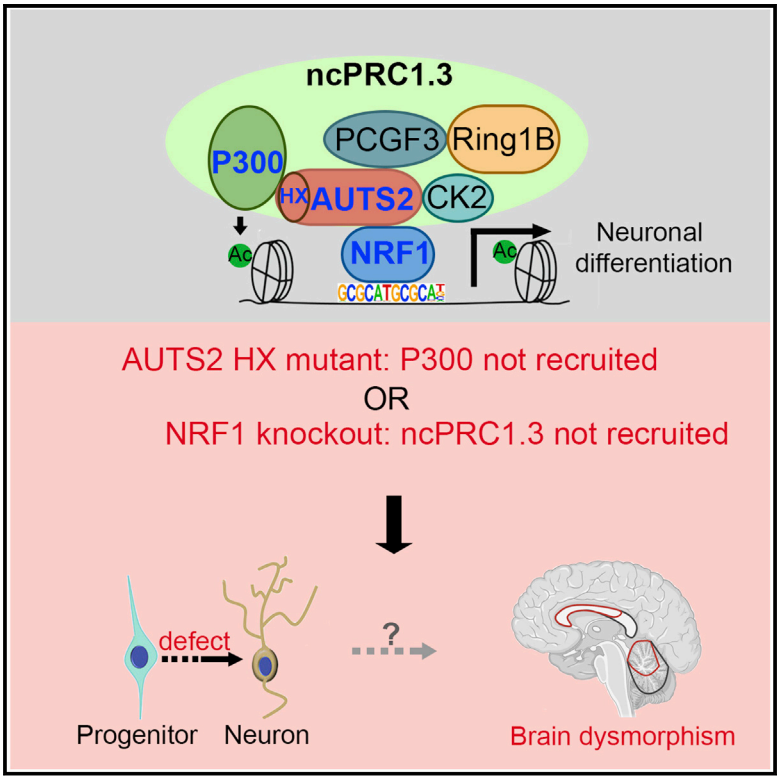

Highlights

- The AUTS2 HX repeat recruits P300 for ncPRC1.3-mediated transcription activation
- Mutations in the HX repeat phenocopy *CREBBP/EP300* mutations in RSTS
- NRF1 recruits ncPRC1.3, which activates a subset of genes fostering neuronal development
- Recruitment of P300 and ncPRC1.3 is required for neuronal progenitor differentiation

Authors

Sanxiong Liu, Kimberly A. Aldinger, Chi Vicky Cheng, ..., Livia Garavelli, William B. Dobyns, Danny Reinberg

Correspondence

danny.reinberg@nyumc.org

In brief

Liu et al. report that mutations in the HX repeat of AUTS2 derived from affected individuals disrupt its interaction with P300, thwarting AUTS2-ncPRC1.3-mediated active transcription. Such mutations reflect those in P300 proper with respect to RSTS. Moreover, NRF1-mediated AUTS2 recruitment is paramount for activation of AUTS2-ncPRC1.3 targets and brain development.

Liu et al., 2021, Molecular Cell *81*, 1–14
November 18, 2021
https://doi.org/10.1016/j.molcel.2021.09.020

CellPress

Please cite this article in press as: Liu et al., NRF1 association with AUTS2-Polycomb mediates specific gene activation in the brain, Molecular Cell (2021), https://doi.org/10.1016/j.molcel.2021.09.020

Molecular Cell

CellPress

Article

NRF1 association with AUTS2-Polycomb mediates specific gene activation in the brain

Sanxiong Liu,[1,2] Kimberly A. Aldinger,[3] Chi Vicky Cheng,[3] Takae Kiyama,[4,5] Mitali Dave,[3] Hanna K. McNamara,[3] Wukui Zhao,[1] Stefano G. Caraffi,[6] Ivan Ivanovski,[6,7] Edoardo Errichiello,[8] Christiane Zweier,[9] Orsetta Zuffardi,[8] Michael Schneider,[10] Antigone S. Papavasiliou,[11] M. Scott Perry,[12] Jennifer Humberson,[13] Megan T. Cho,[14] Astrid Weber,[15] Andrew Swale,[15,16] Tudor C. Badea,[5,17] Chai-An Mao,[4,5] Livia Garavelli,[6] William B. Dobyns,[3,18] and Danny Reinberg[1,2,19,*]

[1]Department of Biochemistry and Molecular Pharmacology, New York University Langone School of Medicine, New York, NY 10016, USA
[2]Howard Hughes Medical Institute, Chevy Chase, MD 20815, USA
[3]Center for Integrative Brain Research, Seattle Children's Research Institute, Seattle, WA, USA
[4]Ruiz Department of Ophthalmology and Visual Science, McGovern Medical School at The University of Texas Health Science Center at Houston (UTHealth), Houston, TX 77030, USA
[5]National Eye Institute, NIH, Bethesda, MD 20892, USA
[6]Struttura Semplice Dipartimentale di Genetica Medica, Azienda USL-IRCCS di Reggio Emilia, Reggio Emilia, Italy
[7]Institute of Medical Genetics, University of Zürich, Zürich, Switzerland
[8]Dipartimento di Medicina Molecolare, Università di Pavia, Pavia, Italy
[9]Institute of Human Genetics, Friedrich-Alexander-Universität Erlangen-Nürnberg (FAU), Schwabachanlage 10, 91054 Erlangen, Germany
[10]Carle Physicians Group, Section of Neurology, St. Christopher's Hospital for Children, Urbana, IL, USA
[11]Neurology, IASO Children's Hospital, Athens, Greece
[12]Comprehensive Epilepsy Program, Jane and John Justin Neuroscience Center, Cook Children's Medical Center, Fort Worth, TX 76104, USA
[13]Division of Genetics, Department of Pediatrics, University of Virginia Children's Hospital, Charlottesville, VA, USA
[14]GeneDx, Inc., Gaithersburg, MD, USA
[15]Liverpool Women's Hospital, Liverpool, UK
[16]Manchester Centre for Genomic Medicine, Manchester, UK
[17]Research and Development Institute, Transilvania University of Brasov, School of Medicine, Brasov, Romania
[18]Department of Pediatrics (Genetic Medicine), University of Washington, Seattle, WA, USA
[19]Lead contact
*Correspondence: danny.reinberg@nyumc.org
https://doi.org/10.1016/j.molcel.2021.09.020

SUMMARY

The heterogeneous family of complexes comprising Polycomb repressive complex 1 (PRC1) is instrumental for establishing facultative heterochromatin that is repressive to transcription. However, two PRC1 species, ncPRC1.3 and ncPRC1.5, are known to comprise novel components, AUTS2, P300, and CK2, that convert this repressive function to that of transcription activation. Here, we report that individuals harboring mutations in the HX repeat domain of AUTS2 exhibit defects in AUTS2 and P300 interaction as well as a developmental disorder reflective of Rubinstein-Taybi syndrome, which is mainly associated with a heterozygous pathogenic variant in *CREBBP/EP300*. Moreover, the absence of AUTS2 or mutation in its HX repeat domain gives rise to misregulation of a subset of developmental genes and curtails motor neuron differentiation of mouse embryonic stem cells. The transcription factor nuclear respiratory factor 1 (NRF1) has a novel and integral role in this neurodevelopmental process, being required for ncPRC1.3 recruitment to chromatin.

INTRODUCTION

Establishment, maintenance, inheritance, and regulated dissolution of facultative heterochromatin (Trojer and Reinberg, 2007) are key for attaining the distinctive gene expression profiles that arise during differentiation in multicellular organisms. In contrast to chromatin domains engaged in transcription, our previous findings demonstrate that it is the repertoire of repressive chromatin domains that is conveyed to daughter cells upon DNA replication, pointing to their role in preserving a given cell identity during cell division (Escobar et al., 2019, 2021a, 2021b). Formation of facultative heterochromatin during development and its integrity in adulthood depend on the activities of the Polycomb group (PcG) of proteins (Bonasio et al., 2010; Margueron and Reinberg, 2011; Di Croce and Helin, 2013).

Two multisubunit complexes, Polycomb repressive complex 1 and 2 (PRC1 and PRC2, respectively) act in concert to establish facultative heterochromatin (Schuettengruber et al., 2017).

Please cite this article in press as: Liu et al., NRF1 association with AUTS2-Polycomb mediates specific gene activation in the brain, Molecular Cell (2021), https://doi.org/10.1016/j.molcel.2021.09.020

PRC2 comprises EZH1/2, the sole activity that catalyzes mono-, di-, and trimethylation of histone H3 at lysine 27 (H3K27me1, H3K27me2, and H3K27me3, respectively), with chromatin domains comprising H3K27me2/me3 providing the platform for chromatin compaction (Lau et al., 2017; Oksuz et al., 2018; Yu et al., 2019; Kim and Kingston, 2020). PRC1 complexes comprise other subsets of the PcG protein family. We and others have previously characterized at least six heterogeneous PRC1 subcomplexes (PRC1.1–PRC1.6), each of which comprise one of the six PcG ring finger (PCGF1-6) components and all of which comprise RING1A and/or RING1B (Gao et al., 2012; Tavares et al., 2012; Hauri et al., 2016). This array of complexes was broadly classified into two major PRC1 subcomplexes, canonical and non-canonical PRC1, which network with PRC2 in distinct manners.

Canonical PRC1 (cPRC1) comprises one of several CBX proteins that bind to chromatin containing nucleosomes decorated with H3K27me3, resulting in chromatin compaction and, thus, transcription repression (Min et al., 2003; Francis et al., 2004; Gao et al., 2012; Lau et al., 2017; Kim and Kingston, 2020). On the other hand, the RYBP or YAF2 components of noncanonical PRC1 (ncPRC1) stimulate RING1-mediated catalysis of mono-ubiquitination of lysine 119 of histone H2A (H2AK119ub1) (Rose et al., 2016), which correlates with transcription inhibition (Stock et al., 2007; Zhou et al., 2008). ncPRC1 coordinates with PRC2 through the PRC2 accessory protein Jarid2, which interacts with H2AK119ub1 (Kasinath et al., 2021) and also stimulates PRC2 activity (Li et al., 2010; Pasini et al., 2010). Although the joint recruitment of PRC2 with cPRC1 or ncPRC1 is distinct, both versions of PRC1 are found in proximity at select genome-wide regions (Gao et al., 2012; Scelfo et al., 2019). Most importantly, this PRC2/PRC1 network is paramount for fostering the appropriate profiles of facultative heterochromatin evident during development and in adulthood (Margueron and Reinberg, 2011; Aloia et al., 2013; Schuettengruber et al., 2017).

Our previous characterization of PRC1 complexes revealed that a subset of ncPRC1 that comprises PCGF3 (ncPRC1.3) or PCGF5 (ncPRC1.5) unexpectedly contains three non-PcG proteins: AUTS2, casein kinase 2 (CK2), and P300 (Gao et al., 2012, 2014). Remarkably, these factors act in concert to not only subvert the repressive function of ncPRC1.3 or ncPRC1.5 but to convert the respective complex into a transcriptional activator (Gao et al., 2014). Specifically, CK2 phosphorylates the RING1A/B subunit of PRC1, inhibiting its catalysis of H2AK119ub1 and, thus, thwarting repression. AUTS2 interacts with PCGF3/5 and, importantly, recruits P300/CREB binding protein (CBP), a known transcriptional co-activator that conveys histone acetyltransferase activity (Bannister and Kouzarides, 1996; Ogryzko et al., 1996). These findings point to AUTS2 having a profound effect on gene expression in the context of defined aspects of development. Indeed, AUTS2-ncPRC1.3 is important during development of the central nervous system (CNS) as well as in the post-developmental stage (see below). In contrast, AUTS2-ncPRC1.5 appears to function during establishment and maintenance of other cell lineages (unpublished data).

The gene encoding AUTS2 was designated as such based on identification of its translocation in a pair of monozygotic twins who were diagnosed with autism (Sultana et al., 2002), but its role in autism spectrum disorders (ASDs) is still putative. The role of AUTS2 in neurodevelopment has been established more widely by identification of variants in *AUTS2* that are associated with various neurological diseases, including intellectual disability (ID), epilepsy, bipolar disorder, and others (Hattori et al., 2009; Mefford et al., 2010; Elia et al., 2010; Oksenberg and Ahituv, 2013; Beunders et al., 2013; Kapoor et al., 2013; Hori and Hoshino, 2017). A thorough and informative report analyzing AUTS2 chromatin immunoprecipitation sequencing (ChIP-seq) in embryonic day 16.5 (E16.5) mouse forebrain reveals AUTS2 occupancy at gene promoters and enhancers whose function appears to be important during neurodevelopment (Oksenberg et al., 2014) and points to its substantive role in activating genes required for appropriate CNS development and function.

Here we report heterozygous *de novo* variants of *AUTS2* in individuals who exhibit a severe phenotype overlapping that of Rubinstein-Taybi syndrome (RSTS), a neurodevelopmental disorder characterized by distinctive facial features, short stature, and ID (Stevens, 1993; Ajmone et al., 2018). Given that AUTS2 interacts with P300, converting ncPRC1.3 into a transcriptional activator, it is notable that RSTS is mainly associated with heterozygous pathogenic variants in *EP300* or *CREBBP*. Strikingly, we found that the AUTS2 variants are defective in P300 interaction, underscoring the biological relevancy of P300 incorporation into AUTS2-ncPRC1.3 with respect to appropriate neurodevelopment and brain function in human.

We further determined the means by which AUTS2-ncPRC1.3 accesses specific chromatin sites in the brain to facilitate transcription and identified the transcription factor nuclear respiratory factor 1 (NRF1) as being instrumental in this process. Previous studies have implicated NRF1 in mitochondrial biogenesis (Scarpulla, 2011) and retinal development (Hsiao et al., 2013; Kiyama et al., 2018). We found that NRF1 mediates AUTS2-ncPRC1.3 recruitment to a subset of neurodevelopmental genes during differentiation of mouse embryonic stem cells to motor neurons as well as in the mouse brain during early development. These findings expose a novel and key role of NRF1 in facilitating appropriate AUTS2-ncPRC1.3-mediated activation of genes involved in neurodevelopment as a consequence of AUTS2-mediated recruitment of P300.

RESULTS

ncPRC1.3 occupies active genes during early development in the mouse brain

The *Auts2* gene encodes 2 major AUTS2 isoforms in the mouse brain (Hori et al., 2014). The long isoform (AUTS2_L, aa 1–1,261; Figure 1B) arises from the full-length (FL) mouse Auts2 transcript (Auts2-1; Figure 1A), which includes 19 exons. The short isoform (AUTS2_S, aa 458–1,261; Figure 1B; Hori et al., 2014) arises from an Auts2 transcript (Auts2-2; Figure 1A), which initiates from a transcriptional start site near exon 7 and comprises a translational start site in the middle of exon 8. Both AUTS2 isoforms contain a PY motif (PPPY amino acids) and an HX repeat that are located, in the case of AUTS2-L, within its N terminus between two proline-rich regions (PR1 and PR2) (Figure 1B). The

Please cite this article in press as: Liu et al., NRF1 association with AUTS2-Polycomb mediates specific gene activation in the brain, Molecular Cell (2021), https://doi.org/10.1016/j.molcel.2021.09.020

CellPress

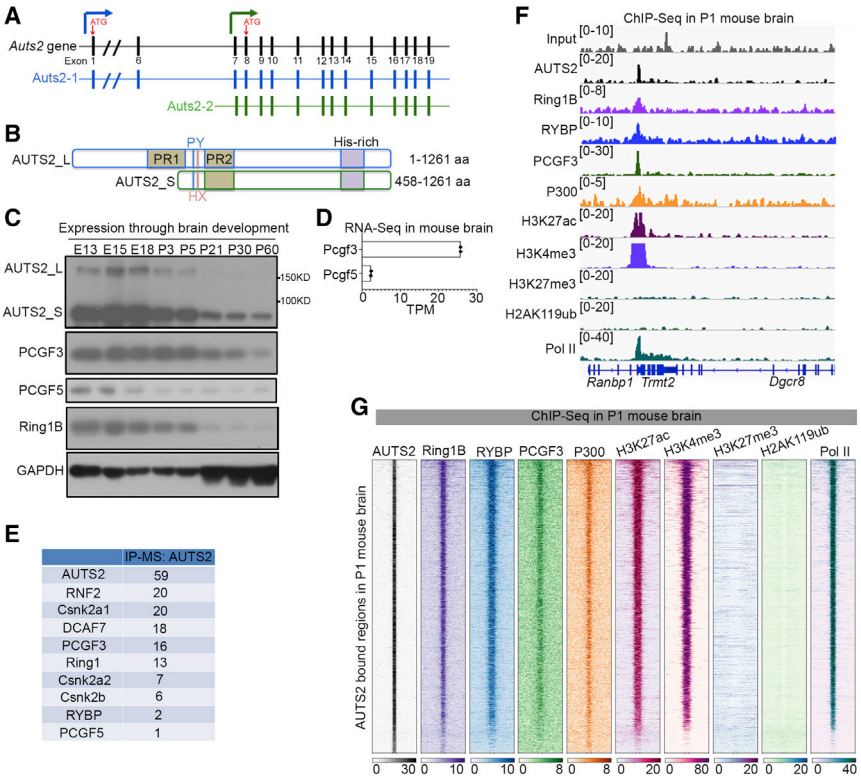

	IP-MS: AUTS2
AUTS2	59
RNF2	20
Csnk2a1	20
DCAF7	18
PCGF3	16
Ring1	13
Csnk2a2	7
Csnk2b	6
RYBP	2
PCGF5	1

Figure 1. AUTS2-ncPRC1.3 targets active genes in the mouse brain

(A) Schematic showing the mouse *Auts2* gene structure and its two major transcripts in the mouse brain. Red arrows indicate the translational start codons used for each AUTS2 isoform.

(B) Schematic showing the domains of the long and short isoforms of mouse AUTS2 protein. PR, proline-rich region; PY, PPPY motif; HX, HX repeat motif comprising alternating HQ (×6) or HT (×3) residues; His-rich, eight histidine repeats.

(C) Expression of AUTS2 and core ncPRC1.3/1.5 components (PCGF3 and PCGF5, respectively, and RING1B) in the mouse brain. Immunoblotting was performed with whole-brain extracts at various developmental stages, as indicated.

(D) Bar graphs showing the value of transcripts per kilobase million (TPM) for Pcgf3 and Pcgf5 revealed by RNA-seq from whole-brain lysate at post-natal day 1 (P1).

(E) Proteomics MS results of immunoprecipitation (IP) using an AUTS2 antibody in whole-brain lysate at P1.

(F) Interactive Genomics Viewer (IGV) browser views showing ChIP-seq for input, AUTS2, RING1B, RYBP, PCGF3, P300, H3K27ac, H3K4me3, H3K27me3, H2AK119ub1, and RNA polymerase II (RNA Pol II) at the representative loci. ChIP-seq was performed in whole-brain lysate at P1.

(G) Heatmap showing AUTS2, RING1B, RYBP, PCGF3, P300, H3K27ac, H3K4me3, H3K27me3, H2AK119ub1, and RNA Pol II ChIP-seq signals centered on AUTS2-bound regions (±5 kb). ChIP-seq was performed in whole-brain lysate at P1.

PY motif is a potential WW domain-binding region in various activating transcription factors (Yagi et al., 1999; Lin et al., 2019). The HX repeat (aa 525–542) comprises alternating HQ (×6) or HT (×3) residues, mutations of which in two other genes (*ATN1* and *RERE*) are related to neurodevelopmental disorders (see Jordan et al., 2018, and Palmer et al., 2019, respectively).

To investigate the role of AUTS2 in brain development, specifically in the context of the ncPRC1.3/1.5 complex, we examined its expression and that of the core PRC1 components in the mouse brain throughout early development. Western blot analysis of whole-mouse-brain lysates using an antibody against the AUTS2 C terminus (aa 1,160–1,259 aa of the human AUTS2 protein; Gao et al., 2014) detected the FL (~170 kDa) and shorter (~95 kDa) isoforms of AUTS2, with the latter being predominant (Figure 1C). Expression of both isoforms decreased gradually throughout early development (Figure 1C). In accordance with this, expression of RING1B and PCGF3 subsided dramatically from post-natal day 5 (P5) (Figure 1C), as did that of PCGF5 (Figure 1C; see also below).

Because AUTS2 is incorporated into ncPRC1.3 comprising PCGF3 and ncPRC1.5 comprising PCGF5 in 293 T-REx cells (tetracycline-controlled Tet-On gene expression systems, Gao et al., 2012), we examined expression of PCGF3 and PCGF5 in whole-brain lysates at P1. RNA sequencing (RNA-seq) data revealed that *Pcgf3*, but not *Pcgf5*, was expressed predominantly in the mouse brain (Figure 1D). Following co-immunoprecipitation (coIP) experiments using an AUTS2 antibody and whole-brain lysate, mass spectrometry (MS) revealed considerably more peptides from PCGF3 than from PCGF5 (Figure 1E). Two other ncPRC1.3 components, RING1A/B and CK2, were also observed (Figure 1E), as reported previously (Gao et al., 2014). Importantly, brain-specific conditional knockout of *Pcgf3* (*Pcgf3*$^{loxp/loxp}$:*Nes*^{Cre}) caused lethality (data not shown), suggesting a critical role of AUTS2-ncPRC1.3 during early brain development.

We next characterized the genomic localization of AUTS2, P300, and the RING1B, RYBP, and PCGF3 components of ncPRC1.3 using ChIP-seq in whole-brain lysate at P1. Consistent with our previous ChIP-seq data of the mouse brain (Gao et al., 2014), AUTS2 associated with ncPRC1.3 components, including P300 in the promoter of active genes that were devoid of histone post-translational modifications (hPTMs) associated with transcription repression, and instead exhibited strong signals for those associated with active transcription; e.g., H3K27ac and H3K4me3 (Figure 1F). Genome-wide analysis (Figure 1G) corroborated this finding and provided strong evidence that AUTS2-ncPRC1.3 is involved in active transcription in the mouse brain. Gene ontology (GO) analysis revealed that terms related to RNA processing and neuronal development were enriched in genes within AUTS2-bound regions (Figure S1).

Individuals with mutations in the *AUTS2* HX repeat share features with RSTS

We reported previously that a truncated form of AUTS2 (aa 404–913) is sufficient to mediate transcription activation through its recruitment of P300 (Gao et al., 2014). However, the AUTS2

Please cite this article in press as: Liu et al., NRF1 association with AUTS2-Polycomb mediates specific gene activation in the brain, Molecular Cell (2021), https://doi.org/10.1016/j.molcel.2021.09.020

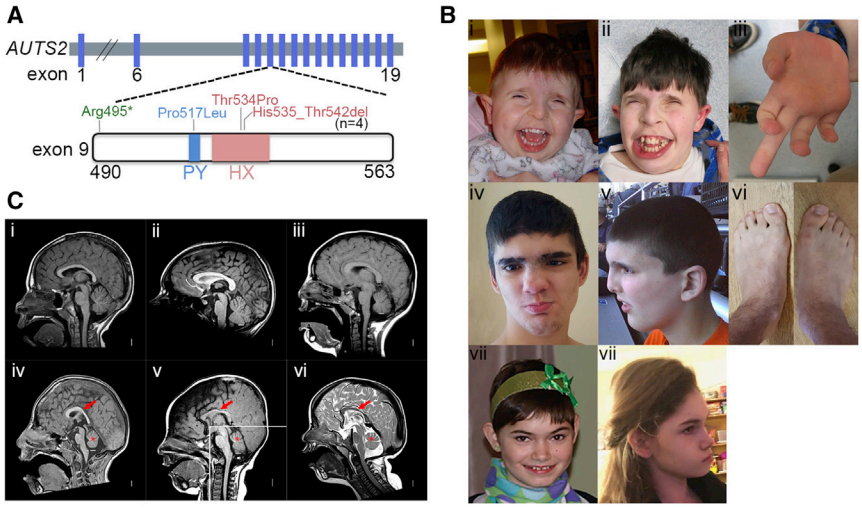

Figure 2. Individuals with mutations in the AUTS2 HX repeat have features overlapping those of RSTS

(A) Schematic illustrating mutations in the *AUTS2* gene from individuals as identified through trio-based exome sequencing. Mutations resulting in similar clinical features are labeled with same color.

(B) Clinical features of individuals with mutations in the AUTS2 PY motif and HX repeat domain. Frontal photos of our original proband (LR05-007 with p.Thr534Pro mutation) at ~1 (i) and 13 (ii) years show reflexive eye closure with smiling as well as a low hanging columella, features often seen in RSTS (i and ii). A photo of his right hand shows severe symphalangism of the right third finger (iii). Frontal (iv) and profile (v) photos of a boy (LR15-003 with p.His535_Thr542 del) at 17 years show thick horizontal eyebrows with synophrys, a prominent (high) nasal bridge, a broad nose with a mildly low columella, and a posteriorly rotated left ear. Photos of his feet show mildly broad halluces (vi). Frontal (vii) and profile (viii) photos of a girl (LR15-004 with p.Pro517Leu) show a normal facial appearance.

(C) Magnetic resonance images from 5 individuals with missense variants in AUTS2 exon 9 and a normal control. The three midline sagittal images in the top row from a normal control (i), a girl with a missense variant (p. Pro517Leu) (ii), and a boy with the recurrent insertion or deletion (indel) (p.His535_Thr542 del, iii) respectively, show normal midline structures. The three midline sagittal images in the bottom row are from a boy with a missense mutation (p.Thr534Pro, iv) and two boys with the recurrent indel (p.His535_Thr542 del, v and vi). All three show a thin and dysplastic CC and small cerebellar vermis (arrows and asterisks, respectively, in iv–vi). The horizontal white or black lines mark the level of the obex, the usual lower extent of the vermis.

residues key for its interaction with P300 and the physiological relevance of this interaction during brain development have remained largely unexplored. In this regard, and as part of an ongoing effort to identify genetic variants associated with developmental brain disorders (Aldinger et al., 2019), we discovered a novel *de novo* missense variant in *AUTS2*. This missense variant was detected in a boy with multiple congenital anomalies and a proposed diagnosis of RSTS. His phenotype was more severe than the syndrome reported previously among individuals with heterozygous *AUTS2* deletions (Beunders et al., 2013). To investigate the clinical phenotype associated with *AUTS2* mutations, we identified 6 additional individuals with *de novo* intragenic variants clustered in exon 9 of *AUTS2* (GenBank: NM_015570.2) (Figures 2A and S2; Table S1). All 7 individuals displayed dysmorphic features and feeding difficulties in infancy, and most had moderate to severe ID and hypotonia (Table S1). Importantly, 5 of these individuals had severe phenotypes (Table S1) and harbored mutations within the HX repeat domain (aa 525–542), which comprises alternating HQ (×6) or HT (×3) residues. Our original proband (LR05-007) had a missense mutation, p.Thr534Pro, whereas the remaining four individuals (LR15-003, LR18-404, LR19-314, and LR19-506) had an identical recurrent small deletion within exon 9: p.His535_Thr542del (Figure 2A).

All 5 individuals with mutations in the HX repeat of AUTS2 had a dysmorphic facial appearance dominated by features seen in RSTS, although less severe than classic RSTS (Table S1). RSTS is a complex multiple congenital anomaly syndrome characterized by short stature, distinctive facial features, and varying degrees of ID (Rubinstein and Taybi, 1963; Wiley et al., 2003). A clinical diagnosis of RSTS was suggested for 2 of the 5 individuals prior to genetic testing (Figure 2B; Table S1). The two other individuals with mutations outside of the HX repeat domain did not exhibit a phenotype overlapping that of RSTS (Figure 2B; Table S1) but instead displayed other neurological defects. Moreover, neuroimaging studies from 4 of the 5 individuals with mutations in the HX repeat showed hypoplasia of the corpus callosum (n = 3), cerebellar hypoplasia and a small posterior fossa (n = 4), and Chiari malformation type 1 (n = 1) (Figure 2C; Table S1). Such brain malformations are also reported in individuals with classic RSTS (Cantani and Gagliesi, 1998; Ajmone et al., 2018). Given that RSTS in most individuals is associated with mutations in *CREBBP* or *EP300* or a microdeletion of 16p13.3 that includes *CREBBP* (Stevens, 1993), we hypothesized that the HX repeat in AUTS2 coordinates with CBP/P300 in regulating proper gene expression in the brain.

Integrity of the HX repeat in AUTS2 and ncPRC1.3/1.5 is required for P300 recruitment and transcription activation

That AUTS2 interacts with P300 in the context of ncPRC1.3 and that mutations in the AUTS2 HX repeat or CBP/P300 are associated with RSTS pointed to AUTS2-HX mutants being defective in P300 interaction. To examine this possibility, we initially expressed FLAG-tagged AUTS2, wild-type (WT) or mutant forms derived from affected individuals, including two variants within the HX repeat (T534P and aa 535–542 deletion) and one outside of this region (P517L within the PY motif), in 293 T-REx cells (Figures 3A and 2A). Strikingly, coIP experiments using FLAG-WT or FLAG mutant AUTS2 revealed that both mutations within the HX repeat (T534P and aa 535–542 deletion), but not P517L, disrupted interaction with P300 (Figure 3B). This finding is in accordance with the clinical diagnosis of RSTS for individuals harboring mutations within the HX repeat but not the P517L

Please cite this article in press as: Liu et al., NRF1 association with AUTS2-Polycomb mediates specific gene activation in the brain, Molecular Cell (2021), https://doi.org/10.1016/j.molcel.2021.09.020

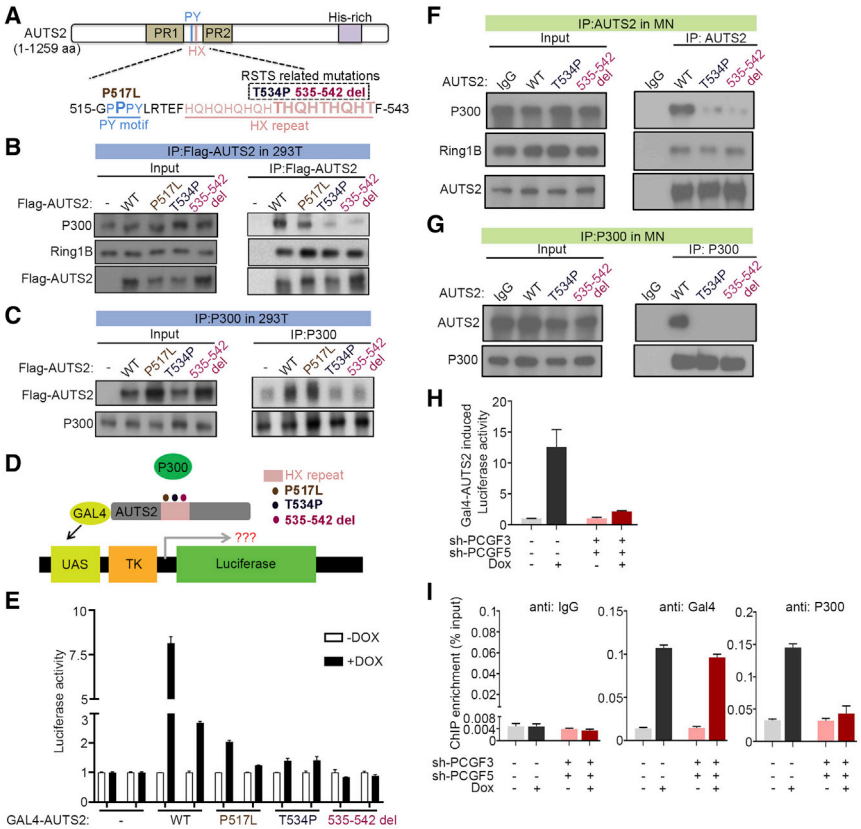

Figure 3. The HX repeat domain and ncPRC1.3/1.5 core components are required for efficient P300 recruitment and transcriptional activation

(A) Schematic showing human AUTS2 variants constructed and expressed in 293 T-REx cells.

(B and C) Western blots showing coIP results from nuclear extract of 293 T-REx cells expressing FLAG-AUTS2, WT or mutant versions, as indicated, using a FLAG antibody (B) or reciprocal IP using a P300 antibody (C).

(D) Schematic of the reporter construct for the luciferase assay in the context of GAL4-AUTS2, WT or mutant versions, as indicated.

(E) Luciferase activity in cells expressing GAL4-AUTS2, WT or mutant versions, before and after doxycycline treatment.

(F and G) Western blots showing coIP results from nuclear extract of MNs differentiated from WT and *Auts2* HX mutant (T534P and aa 535–542 deletion, respectively) mESCs, as indicated, using an AUTS2 antibody (F) or reciprocal IP using a P300 antibody (G).

(H) Luciferase activity in cells expressing GAL4-AUTS2 in the presence or absence of PCGF3 and PCGF5 before and after doxycycline treatment.

(I) ChIP-qPCR at the UAS element using the antibodies as indicated in cells expressing GAL4-AUTS2 in the presence or absence of PCGF3 and PCGF5 before and after doxycycline treatment.

mutation (Table S1). The WT and all AUTS2 variants interacted stably with RING1B (Figure 3B), suggesting that AUTS2 regions outside of the PY motif and HX repeat could mediate AUTS2 incorporation into ncPRC1. Importantly, reciprocal coIP experiments against endogenous P300 confirmed that AUTS2 mutated in its HX repeat disrupted P300 interaction (Figure 3C). Similar results were observed using a more biologically relevant system: cells undergoing differentiation into motor neurons (see below).

Because P300 is required for AUTS2-mediated transcriptional activation (Gao et al., 2014), we tested AUTS2 HX mutants for the ability to activate transcription. GAL4–AUTS2, WT or mutant in the PY motif or the HX repeat, or GAL4 alone were inducibly expressed in 293 T-REx cells containing an integrated luciferase reporter with an upstream activating sequence (UAS) element comprising five consecutive GAL4 DNA binding sites (Figure 3D). Indeed, the GAL4-AUTS2 mutants in the HX repeat exhibited a severe defect in doxycycline-mediated induction of luciferase activity compared with the WT (Figure 3E). Although the mutation in the PY motif did not appear to affect AUTS2-P300 interaction (Figures 3B and 3C), it did attenuate AUTS2-mediated transcriptional activation (Figures 3D and 3E). Because the PY motif associates with WW domain-containing proteins to facilitate transcriptional activation (Yagi et al., 1999; Lin et al., 2019), the integrity of the PY motif and the HX repeat may be required for AUTS2-induced gene activation.

To corroborate the critical role of the HX repeat domain in mediating AUTS2-P300 interaction, we sought a more relevant system: *in vitro* neuronal differentiation (see below). We genetically modified mouse embryonic stem cells (mESCs) to harbor one of two mutations derived from affected individuals in the HX repeat of the endogenous *Auts2* locus (T534P or aa 535–542 deletion; Figures S3A and S3B, respectively), which could then be differentiated toward motor neurons (see Figure 5A for more details). Expression levels of AUTS2 were unaffected by either mutation (Figure S3C). Consistent with our observations in 293T cells, both mutations of the HX repeat domain of AUTS2 disrupted its interaction with P300 but not its incorporation into the ncPRC1 complex (Figures 3F and 3G).

Because AUTS2 associates with ncPRC1.3/1.5 core components and with P300 (Gao et al., 2012, 2014), we wondered whether PRC1 core components are required for efficient P300 recruitment and transcription activation. Indeed, shRNA-mediated silencing of PCGF3 and PCGF5 (Figure S3D) led to a dramatic loss in GAL4-AUTS2-mediated activation of the luciferase reporter (Figure 3H) and recruitment of P300 to the promoter of the reporter (Figure 3I). These results establish that the AUTS2 HX repeat domain and ncPRC1.3/1.5 core components engage in efficient P300 recruitment for transcription activation.

Our results so far underscore that the context in which P300 functions (i.e., ncPRC1.3) is of prime importance and likely relevant in the case of individuals who express the AUTS2 HX repeat mutants reported above and exhibit RSTS, a syndrome associated previously with CBP/P300 mutations (Stevens, 1993). As shown above, these AUTS2 mutants thwart P300 interaction, essentially rendering ncPRC1.3 target genes defective in P300-mediated activation. To understand the role of ncPRC1.3

Please cite this article in press as: Liu et al., NRF1 association with AUTS2-Polycomb mediates specific gene activation in the brain, Molecular Cell (2021), https://doi.org/10.1016/j.molcel.2021.09.020

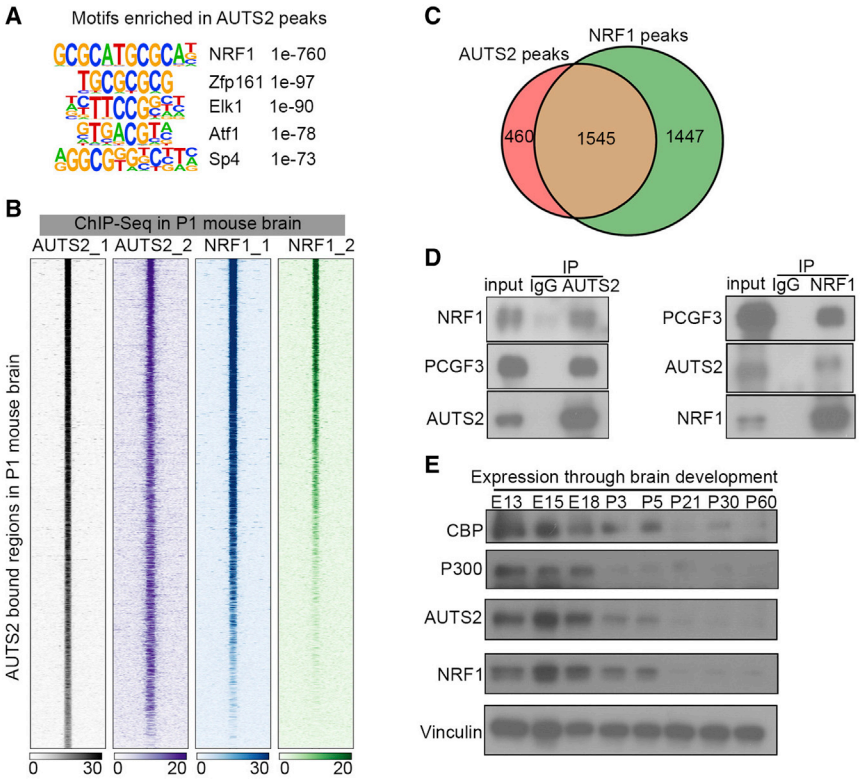

Figure 4. The TF NRF1 colocalizes with AUTS2 on chromatin and interacts physically with AUTS2 in the mouse brain

(A) Top 5 enriched motifs identified in AUTS2-bound regions in mouse brain using HOMER.

(B) Heatmap showing AUTS2 and NRF1 ChIP-seq signals centered on AUTS2-bound regions (±5 kb) with two replicates. ChIP-seq was performed in whole-brain lysate at P1.

(C) Venn diagram showing the extent of overlap for AUTS2- and NRF1-bound regions revealed by ChIP-seq from (B).

(D) Reciprocal coIP and western blot analyses demonstrating AUTS2 and NRF1 interaction in whole-brain lysate at P1.

(E) Expression of CBP, P300, AUTS2, and NRF1 in the mouse brain. Immunoblotting was performed with whole-brain extracts at various developmental stages, as indicated.

in fostering appropriate P300 activity during neurodevelopment, we next sought the means by which ncPRC1.3 accesses its target genes and the importance of this process for appropriate neurodevelopment.

AUTS2 and NRF1 co-localize within chromatin and interact in the mouse brain

To identify the factor(s) involved in the key process by which AUTS2 accesses chromatin, we first determined the motifs of transcription factors (TFs) enriched in AUTS2-bound sites in the mouse brain and identified an overrepresentation for that of NRF1 (Figure 4A). NRF1 is a TF involved in mitochondrial biogenesis (Scarpulla, 2011), which binds to GC-rich DNA elements in the promoters of many mitochondrial biogenesis-related genes (Evans and Scarpulla, 1990; Gleyzer et al., 2005). NRF1 is also associated with regulation of neurite outgrowth (Chang et al., 2005; Tong et al., 2013) and has essential roles in retinal development (Hsiao et al., 2013; Kiyama et al., 2018), but its function and regulation in the CNS are largely unknown. To validate our computational prediction, we performed ChIP-seq for NRF1 using 2 different antibodies and lysates from whole mouse brain and ascertained that the majority of AUTS2 peaks (1,545 of 2,005 total peaks) were associated with NRF1 binding (Figures 4B and 4C).

Based on this high overlap between chromatin-bound AUTS2 and NRF1, we next tested the possibility that NRF1 might physically interact with AUTS2. Reciprocal coIP assays using nuclear extracts from whole mouse brain revealed that, indeed, endogenous NRF1 and AUTS2 were associated physically (Figure 4D). Notably, the core component of AUTS2-ncPRC1.3, PCGF3, also co-immunoprecipitated with NRF1, indicating that AUTS2 interaction with NRF1 occurred in the context of the ncPRC1.3 complex in the mouse brain (Figure 4D). Moreover, the interaction between AUTS2 and NRF1 was independent of the AUTS2 HX repeat domain (Figure S3E). Interestingly, expression of NRF1 recapitulated the pattern of AUTS2-ncPRC1.3 and CBP/P300 expression during early brain development (Figures 4E and 1C). These data strongly suggest that NRF1 contributes to recruitment of AUTS2 and its associated ncPRC1 complex, although it is also clear that both have independent targets, likely because of their additional functions and partnership with other factors.

AUTS2 and NRF1 colocalize with ncPRC1.3 at actively transcribed loci in motor neurons

We next gauged the profile of chromatin binding and transcription regulation inherent to AUTS2-ncPRC1.3 and NRF1 in the context of a system by which differentiated motor neurons (MNs) are attained (Wichterle et al., 2002; Mazzoni et al., 2013; Narendra et al., 2015). Under these conditions, expression of AUTS2 and PCGF3 was upregulated significantly in MNs, whereas that of NRF1 decreased by half at the protein (Figure 5A) and RNA levels (Figure S4A). In contrast, the overall levels of the PRC1 complex as reflected by that of RING1B were downregulated (Figures 5A and S4A), consistent with its essential role in maintaining mESC identity (Endoh et al., 2008). To complement our previous ChIP-seq for RNA polymerase II (RNA Pol II) in mESCs and MNs (Narendra et al., 2015; LeRoy et al., 2019), we performed similar ChIP-seq for AUTS2 and NRF1. The majority of regions that gained AUTS2 binding upon MN differentiation also accumulated NRF1 binding (Figure 5B). Importantly, these regions became actively transcribed during differentiation, as evidenced by increased RNA Pol II binding (Figure 5B).

To examine whether AUTS2 cooperates with ncPRC1.3 for active transcription in MNs, we analyzed the genome-wide

Please cite this article in press as: Liu et al., NRF1 association with AUTS2-Polycomb mediates specific gene activation in the brain, Molecular Cell (2021), https://doi.org/10.1016/j.molcel.2021.09.020

CellPress

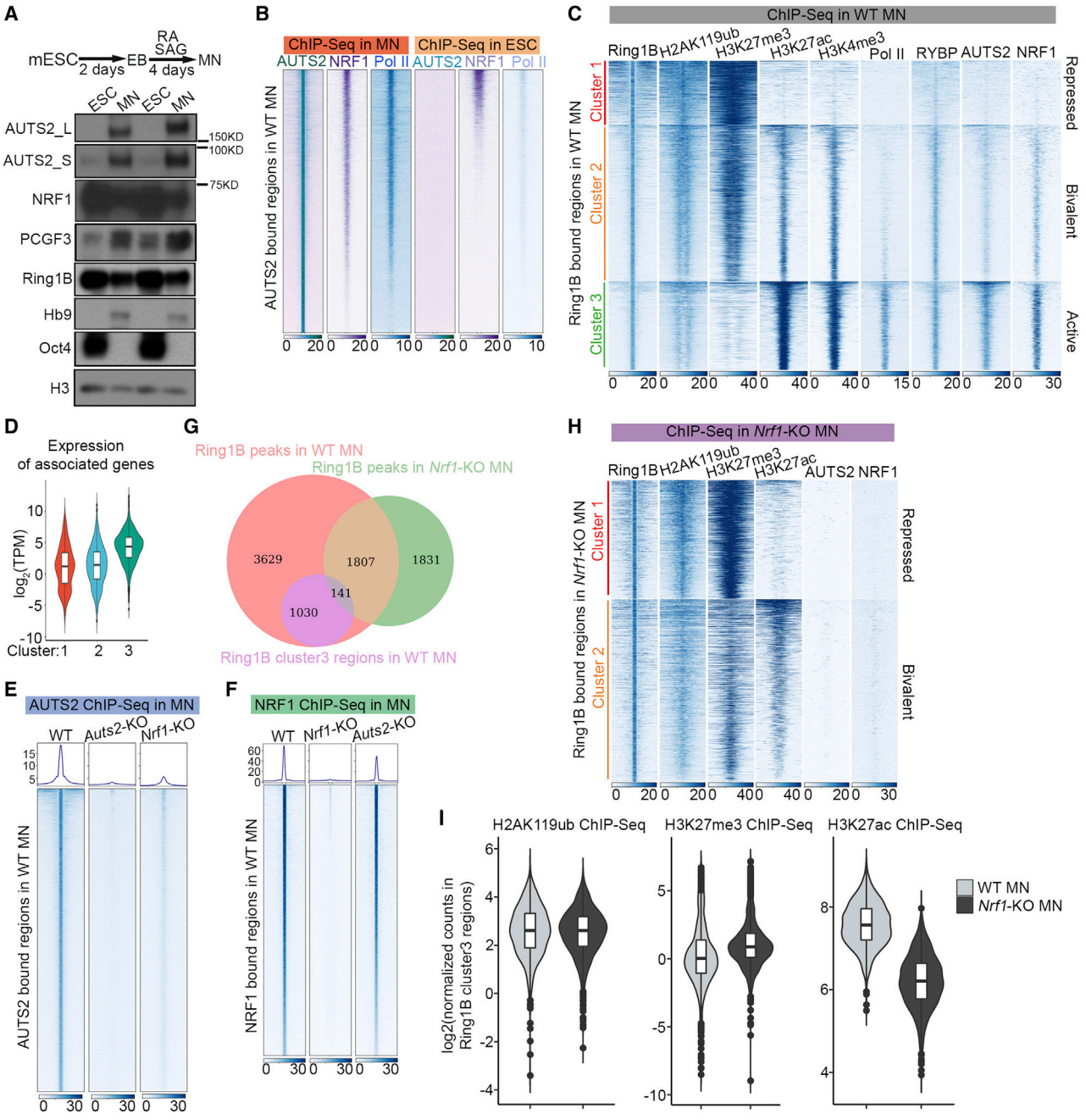

Figure 5. NRF1 is crucial for AUTS2-ncPRC1.3-associated active transcription in MNs

(A) The schematic at the top depicts the protocol for differentiation of mouse embryonic stem cells (mESCs) into motor neurons (MNs) using retinoic acid (RA) and smoothened agonist (SAG). EB, embryoid body. Bottom: western blot showing expression of AUTS2, NRF1, PCGF3, and RING1B in mESCs and MNs.

(B) Heatmap showing AUTS2, NRF1, and RNA Pol II ChIP-seq signals centered on AUTS2-bound regions identified in WT MNs (±5 kb).

(C) k-means clustering of RING1B, H2AK119ub1, H3K27me3, H3K27ac, H3K4me3, RNA Pol II, RYBP, AUTS2, and NRF1 ChIP-seq signals from WT MNs centered on RING1B-bound regions identified in WT MNs (±5 kb).

(D) Violin plot of the $\log_2$(TPM) of genes assigned to each cluster (as indicated in C), quantified from RNA-seq of WT MNs.

(E) Average density profiles (top) and heatmap (bottom) showing AUTS2 ChIP-seq signals from WT, *Auts2* KO, and *Nrf1* KO MNs centered on AUTS2-bound regions identified in WT MNs (±5 kb).

(F) Average density profiles (top) and heatmap (bottom) showing NRF1 ChIP-seq signals from WT, *Nrf1* KO, and *Auts2* KO MNs centered on NRF1-bound regions identified in WT MNs (±5 kb).

(G) Venn diagram showing the extent of overlap for RING1B-bound regions in WT MNs, RING1B cluster 3 regions (as indicated in C), and RING1B-bound regions in *Nrf1* KO MNs revealed by ChIP-seq.

(legend continued on next page)

Please cite this article in press as: Liu et al., NRF1 association with AUTS2-Polycomb mediates specific gene activation in the brain, Molecular Cell (2021), https://doi.org/10.1016/j.molcel.2021.09.020

distribution of a set of hPTMs (H2AK119ub1, H3K27me3, H3K27ac, and H3K4me3) and the core ncPRC1 subunits RING1B and RYBP. Consistent with studies in other systems (Kloet et al., 2016; Cohen et al., 2018; Loubiere et al., 2020), k-means clustering revealed three discrete classes of RING1B-bound regions in MNs (Figure 5C). In cluster 1, we observed strong and broad ChIP-seq signals for RING1B, H2AK119ub1, and H3K27me3 and absence of signals for H3K27ac, H3K4me3, RNA Pol II, and the ncPRC1 component RYBP/YAF2 (RYBP antibodies do not distinguish RYBP and YAF2), suggesting that these regions are co-repressed by PRC2 and cPRC1. The second cluster exhibited lower levels of H2AK119ub1 and H3K27me3 and increased levels of H3K27ac and H3K4me3, mostly abundant at the peak center, suggesting that these RING1B-bound regions featured bivalency (Bernstein et al., 2006; Voigt et al., 2013). The third cluster exhibited H3K27ac- and H3K4me3-marked active regions enriched for developmental GO terms (Figure S4B). AUTS2 and NRF1 binding were enriched specifically in cluster 3, which also exhibited elevated levels of the ncPRC1 components RYBP/YAF2 (Figure 5C). Accordingly, genes flanking cluster 3 regions were expressed at levels significantly higher than those in clusters 1 and 2 (Figure 5D). These data strongly suggest that NRF1 associates with AUTS2-ncPRC1 to facilitate transcription in MNs.

NRF1 directs AUTS2-ncPRC1 chromatin binding

To ascertain whether AUTS2 binding to chromatin is dependent on NRF1 or vice versa, we first performed ChIP-seq for the presence of AUTS2 or NRF1 as a function of NRF1 or AUTS2 depletion, respectively. Exon 9 of the *Auts2* gene was targeted by CRISPR-Cas9 to remove the long and short forms of the protein (Figures S4C–S4E; Table S2), whereas exon 4 of the *Nrf1* gene was targeted by CRISPR-Cas9 to remove NRF1 protein (Figures S4F–S4H; Table S2) in mESCs from which MNs were then derived. As a consequence of NRF1 depletion, AUTS2 binding at most of its targets was decreased in MNs (Figures 5E and S5A). However, NRF1 ChIP-seq signals remained largely unaltered upon AUTS2 depletion (Figures 5F and S5B), demonstrating that, although AUTS2 binding is NRF1 dependent, NRF1 binding to chromatin is AUTS2 independent.

We next probed how NRF1-directed AUTS2 binding might modulate ncPRC1.3-associated active transcription. Under NRF1-depleted conditions, we performed ChIP-seq for RING1B and a set of hPTMs (H2AK119ub1, H3K27me3, and H3K27ac), followed by k-means clustering analysis. Remarkably, Ring1B binding in the NRF1 knockout (KO) MNs was lost at the majority of cluster 3 regions (1,030 of 1,171 peaks) found in the WT (Figure 5G). Moreover, we did not recover the cluster of RING1B-bound active regions (labeled by H3K27ac but not by H3K27me3 or H2AK119ub1) relative to the control (Figures 5H and 5C), strongly suggesting that the absence of NRF1 was detrimental to ncPRC1.3-mediated active transcription. As evident in Figure 5C, the H3K27ac signal at cluster 3 regions was reduced dramatically in NRF1-KO MNs, whereas the H3K27me3 signal was increased (Figure 5I). Collectively, these data demonstrate a pivotal role of NRF1 in facilitating ncPRC1.3-associated active transcription by directing AUTS2 binding to chromatin in MNs.

We attempted to delete NRF1 in the mouse brain from the embryonic stage to validate the NRF1-mediated AUTS2 recruitment we observed in cell culture, but such embryos did not survive, consistent with a previous report showing that *Nrf1*-null mouse embryos die between E3.5 and E6.5 (Huo and Scarpulla, 2001). Instead, we chose the $Tbr1^{CreERT2}$ line to strategically delete *Nrf1* in the adult mouse brain to examine its role in the CNS (Figures S6A–S6C, see STAR Methods for details). Importantly, we noticed several histological anomalies in these mutant mice ($Tbr1^{CreERT2/+}$: $Nrf1^{fx/fx}$: $Pou4f1^{CKO/+}$) compared with control mice ($Tbr1^{CreERT2/+}$: $Nrf1^{fx/+}$: $Pou4f1^{CKO/+}$), including a reduction in the size of the hippocampus and the width of the corpus callosum as well as an enlarged lateral ventricle, indicating neuronal loss in the cortex and hippocampus (Figures S6D and S6E). A significant loss of retinal ganglion cells (RGCs) was observed in retinas collected from these mutant mice (Figures S6F and S6G), consistent with its previously elucidated function in retinal development (Kiyama et al., 2018).

The HX repeat in AUTS2 and NRF1-directed binding is required for PNP-to-MN differentiation

That AUTS2 and NRF1 might coordinately regulate the process of neuronal differentiation has not been recognized previously. Thus, we next characterized gene expression profiles during the transition from multipotent posterior neural progenitors (PNPs) to terminally differentiated MNs as a function of the presence of AUTS2 or NRF1. We performed single-cell RNA-seq (scRNA-seq) on MNs differentiated from mESCs under conditions of *Auts2* KO, mutations in the AUTS2 HX repeat (*Auts2*-HX*, aa 535–542 deletion), or *Nrf1* KO (STAR Methods) compared with the WT. We obtained 816 high-quality (cells with more than 3,000 detected genes) single-cell transcriptomes from all samples (WT, 228 cells; *Auts2* KO, 221 cells; *Auts2*-HX*, 184 cells; *Nrf1* KO, 183 cells) for in-depth analyses (Figures 6A and S7A). To identify major cell types, we performed unsupervised clustering on a graph-based representation of the cellular transcriptomes. 5 major clusters were visualized in uniform manifold approximation and projection (UMAP) embedding (Butler et al., 2018; Becht et al., 2018), as represented by color-coded dashed circles (Figure 6A). Clusters were annotated according to known markers and previously established lineage information (Wichterle et al., 2002; Briggs et al., 2017); i.e., PNPs expressing *Sox3*, posterior and ventral neural progenitors (PVNPs) expressing *Hoxd4*, newborn MN (NMNs) expressing *Neurog2*, and MNs expressing *Mnx1* and *Chat* (Figures S7B and S7C). Importantly, cells from all samples were clustered by cell type identity rather than sample identity (Figure 6A), indicating little or no batch effect. *Auts2* and *Nrf1* were highly

(H) k-means clustering of RING1B, H2AK119ub1, H3K27me3, H3K27ac, AUTS2, and NRF1 ChIP-seq signals from *Nrf1* KO MNs centered on RING1B-bound regions identified in *Nrf1* KO MNs (±5 kb).

(I) Violin plot of the $\log_2$(normalized counts), quantified from H2AK119ub, H3K27me3, and H3K27ac ChIP-seq signal at RING1B cluster 3 regions (as indicated in C) in WT and *Nrf1* KO MNs.

Please cite this article in press as: Liu et al., NRF1 association with AUTS2-Polycomb mediates specific gene activation in the brain, Molecular Cell (2021), https://doi.org/10.1016/j.molcel.2021.09.020

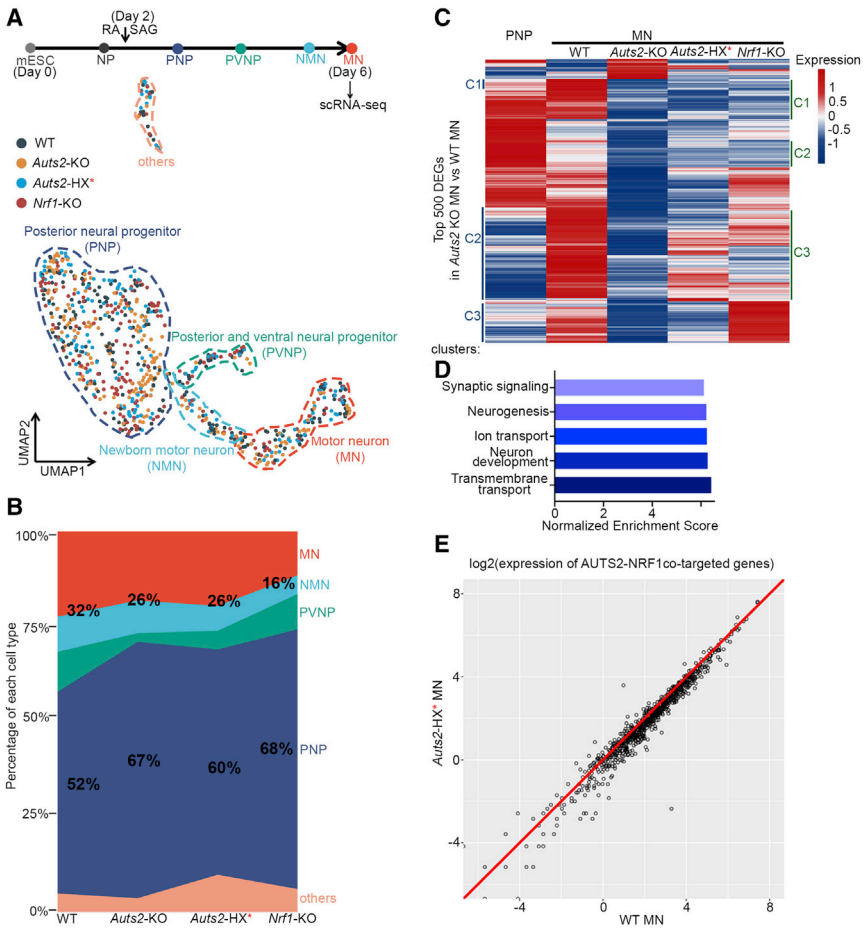

Figure 6. Defect in PNP-to-MN differentiation under *Auts2* KO, mutation in the *Auts2* HX repeat, or *Nrf1* KO as revealed by scRNA-seq

(A) The schematic at the top depicts cell lineage transitions from mESCs to MNs. MNs (day 6) differentiated from WT, *Auts2* KO, *Auts2* HX mutant (aa 535–542 deletion), and *Nrf1* KO ESCs were harvested for scRNA-seq. Bottom: dimensionality reduction (UMAP) of 816 cells from WT, *Auts2* KO, *Auts2* HX mutant, and *Nrf1* KO samples, sequenced with the Smart-seq3 technique and colored by sample identity (WT, 228 cells; *Auts2* KO, 221 cells; *Auts2*-HX*, 184 cells; *Nrf1* KO, 183 cells). Five cell classes revealed by unsupervised clustering of cellular transcriptomics are represented by color-coded circles of dashed lines and annotated based on marker gene expression. The colors of the dashed lines match those for the cell types shown at the top.

(B) Proportional stacked area graph showing the abundance of each cell type in MNs differentiated from WT, *Auts2* KO, *Auts2* HX mutant (aa 535–542 deletion), and *Nrf1* KO ESCs. The percentages of MNs (MN and NMNs) and PNPs in each sample are labeled.

(C) The top 500 DEGs were identified by comparing *Auts2* KO MNs with WT MNs. Expression of these DEGs across WT PNPs, WT MNs, *Auts2* KO MNs, *Auts2* HX mutant MNs, and *Nrf1* KO MNs is shown by a heatmap. The color scale represents the averaged and scaled expression values from each cell population. Labeling of clusters (C1, C2, and C3) on left is based on gene expression differences in WT PNPs, WT MNs, and *Auts2* KO MNs. Labeling of clusters (C1, C2, and C3) on the right is based on gene expression differences in WT MNs, *Auts2* KO MNs, and *Nrf1* KO MNs.

(D) Bar plot summarizing results of GO analysis for genes downregulated in *Auts2* KO MNs versus WT MNs.

(E) Scatterplot of $\log_2$(normalized expression of AUTS2-NRF1 co-targeted genes) in WT and *Auts2* HX mutant MNs from scRNA-seq.

expressed in all cell types (Figure S7C), suggesting their involvement in all of the different stages of differentiation.

To pursue the potential functional requirement of the intact HX repeat in AUTS2 and of NRF1 for proper MN differentiation, we first compared the percentage of MNs (including NMNs and MNs) and PNPs under WT, *Auts2* KO, Auts2-HX*, and *Nrf1* KO conditions. The percentage of PNPs was retained at a much higher level in the case of either mutant (52% in the WT compared with 67% in *Auts2* KO, 60% in *Auts2*-HX*, and 68% in *Nrf1* KO; Figure 6B). Moreover, we observed a slight decrease in the percentage of MNs in *Auts2* KO and *Auts2*-HX* (32% in the WT, 26% in *Auts2* KO and *Auts2* HX*) and a more severe defect in *Nrf1* KO (32% to 16%) (Figure 6B). The lower percentage of MNs under these mutant conditions was not due to apoptosis (Figure S7D) but, instead, pointed to a defect in PNP differentiation into MNs. To gain more insight into the molecular mechanism by which AUTS2 and NRF1 contribute to the transition from PNPs to MNs, we further analyzed the differentially expressed genes (DEGs) specifically in the MN population from WT or *Auts2* KO (STAR Methods). Among the top 500 DEGs, 458 genes were downregulated in *Auts2* KO (Figure 6C). Strikingly, 405 of these 458 genes were also downregulated in *Auts2*-HX mutant MNs, in accordance with the critical role of the HX repeat domain in mediating AUTS2-P300 interaction and transcriptional activation (Figures 6C and 3B–3G). Furthermore, about half of these 458 genes (205 of 458) were also downregulated in *Nrf1* KO MNs compared with WT MNs (C1, C2, and C3 labeled on the right in Figure 6C). To confirm whether NRF1-directed AUTS2 binding is required for transcriptional activation of AUTS2-ncPRC1.3-associated active genes (cluster 3 region; Figures 5C and 5H), we compared the DEGs in *Nrf1* KO MNs with the genes located in the cluster 3 and cluster 1 regions from the RING1B ChIP-seq. Consistent with KO of *Nrf1* leading to loss of AUTS2-ncPRC1 binding to active genes (Figures 5C, 5G, and 5H), genes located in cluster 3 regions were enriched in the downregulated category in *Nrf1* KO MNs (Figure S8). In contrast, very few of the genes located in the cluster 1 region (co-repressed by cPRC1 and PRC2) were affected in *Nrf1* KO MNs (Figure S8). These results strongly suggest that AUTS2 and NRF1 function coordinately in regulating transcriptional activation (Figures 5C and 5H).

We next asked whether the genes that were downregulated in *Auts2* KO MNs reflected those associated with the transition from PNPs to MNs. Indeed, 186 of the 458 genes were

Please cite this article in press as: Liu et al., NRF1 association with AUTS2-Polycomb mediates specific gene activation in the brain, Molecular Cell (2021), https://doi.org/10.1016/j.molcel.2021.09.020

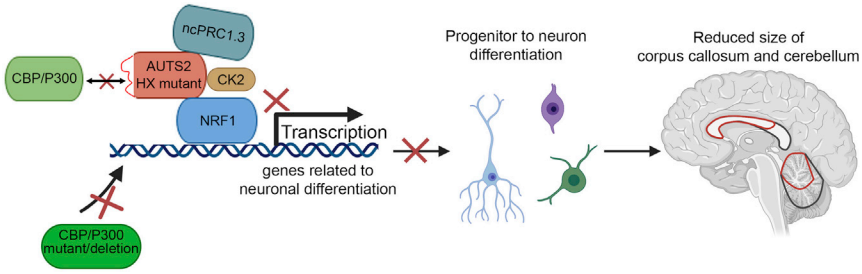

Figure 7. Model: AUTS2-ncPRC1.3 activates its targeted genes for brain development through NRF1-mediated recruitment and HX repeat-mediated P300 interaction

Mutations or deletions of CBP or P300 impede neuronal differentiation during early brain development and result in malformation of several brain regions, including the CC and cerebellum, in individuals with RSTS. As shown here, mutations in the AUTS2 HX repeat domain impair AUTS2 interaction with P300 in the context of ncPRC1.3, effectively disabling transcription activation. We speculate that such disruptions of appropriate gene activation lead to a defect in brain development that overlaps with RSTS.

upregulated normally during PNP-to-MN differentiation in the WT but were defective in activation in *Auts2* KO (C1, C2, and C3 labeled on the left in Figure 6C). For example, upregulation of *Asic2*, a member of the sodium channel superfamily that regulates synaptic function (Zha et al., 2009), and of *Pnpla6*, a phospholipase that functions in neurite outgrowth (Guerreiro et al., 2015), was attenuated significantly under conditions of AUTS2 depletion. Finally, genes that were downregulated in *Auts2* KO MNs were enriched for GO terms related to neuronal differentiation and function (Figure 6D).

We demonstrated that the AUTS2-HX repeat domain and NRF1 are required for AUTS2-mediated transcription activation in the context of ncPRC1.3. Comparison of the expression levels of AUTS2-NRF1 co-targeted genes demonstrated that the vast majority of NRF1/AUTS2 co-targets (674 of 837 genes) were downregulated in AUTS2 HX mutant MN compared with the WT (Figure 6E). These data demonstrate that AUTS2 and NRF1 function coordinately to foster appropriate differentiation of PNPs to MNs by directly binding to and activating a subset of the relevant genes.

DISCUSSION

Our findings support a model in which NRF1 directs AUTS2-ncPRC1.3 binding to a subset of neuronal differentiation-related genes that are subjected to activation by P300 through its interaction with the AUTS2 HX repeat domain (Figure 7). Given the existence of ncPRC1.3, in which AUTS2 conveys transcription activation, along with the reported association of AUTS2 haploinsufficiency in AUTS2 syndrome (Beunders et al., 2013) and possibly in ASD (Sultana et al., 2002), AUTS2 appeared to be key for regulating appropriate neurodevelopment. Here we identified the critical role of its HX repeat domain by interrogating mutations found in individuals exhibiting a distinct and severe neurodevelopmental syndrome that overlaps with RSTS. Although RSTS is largely associated with pathogenic variants in the *EP300*/*CREBBP* genes, the AUTS2-HX mutants associated with affected individuals reported here essentially reflect a defect in P300 function. Our *in vitro* and cell-based studies demonstrated that RSTS-associated AUTS2 mutations in the HX repeat domain disrupt AUTS2-P300 interaction and attenuate AUTS2-mediated active transcription. A recent study reports an individual with a syndromic neurodevelopmental disorder harboring a different mutation (aa 532–541 deletion) in the AUTS2 HX repeat domain (Martinez-Delgado et al., 2021), further pointing to its critical role in normal brain function. Moreover, mutations within exon 9 outside of the HX repeat, such as the PY motif, as well as a mutation at residue 495, result in individuals who display severe behavioral phenotypes, such as epilepsy, in lieu of RSTS (Table S1), further stressing the role of AUTS2 in normal brain function. Interestingly, a recent report shows that AUTS2 controls neuronal differentiation in a PRC1-independent manner through BMP inhibition, pointing to the multifaceted actions of AUTS2 in neurodevelopment (Geng et al., 2021).

Our study directs attention to NRF1 in facilitating chromatin access by AUTS2, key for its role at the appropriate target genes. We found that most AUTS2 binding events require NRF1, whereas most NRF1 binding is AUTS2 independent. A previous report also noted that the motif of NRF1 is enriched significantly in AUTS2-bound regions (Oksenberg et al., 2014), although the enrichment is less dramatic than observed here. On the other hand, a recent study identified the TF USF1/2 as being key for PCGF3 chromatin binding in mESCs (Scelfo et al., 2019), but the motif corresponding to USF1/2 was not recovered in our study, suggesting that cell type/tissue-specific mechanisms might dictate ncPRC1.3 recruitment to chromatin.

Our previous mechanistic findings resolved the means by which the function of ncPRC1.3/1.5 comprising AUTS2, P300, CK2, PCGF3 or PCGF5, RING1A and/or RING1B, and RYBP or YAF2 is converted from a typical PRC1 that facilitates transcription repression to that of a transcriptional activator (Gao et al., 2014). This conversion involves AUTS2-mediated recruitment of P300 and CK2-mediated phosphorylation of serine 168 of the integral PRC1 subunit RING1, which thwarts its catalysis of H2AK119ub1 (Gao et al., 2014). Given that RYBP/YAF2 in other ncPRC1 complexes stimulate such RING1A/RING1B-mediated ubiquitination, their presence in ncPRC1.3 may indicate additional function(s) of these components. Distinct ncPRC1.3/1.5 complexes comprise another non-PcG protein, FBRSL1, which shares a high degree of sequence similarity with AUTS2 (Gao et al., 2012). Interestingly, AUTS2 and FBRSL1 bind competitively to the respective PCGF subunit of ncPRC1.3/1.5 (Gao et al., 2014). Consistent with our data supporting the importance of ncPRC1.3 in neurodevelopment, mutations in FBRSL1 are also associated with a neurodevelopmental syndrome (Ufartes

et al., 2020). However, it has yet to be determined whether FBRSL1-ncPRC1.3 acts in a repressive or activating manner.

As shown here, AUTS2 interacts with P300 through its HX repeat domain, and NRF1 associates with AUTS2, but, intriguingly, AUTS2 and P300 convey efficient transcription activation only in the context of ncPRC1.3/1.5. We speculate that ncPRC1.3 provides a conformational context in which P300 recruitment is facilitated or stabilized and/or its activity is optimized. Perhaps this module exposes an interacting surface(s) for NRF1 as well. The characterization of NRF1 performed by others demonstrates its ability to dimerize and its phosphorylation at several serine residues within its amino terminus (Gugneja and Scarpulla, 1997). These phosphorylation events do not regulate NRF1 dimerization; instead, mutation of these sites compromises NRF1 DNA binding activity (Gugneja and Scarpulla, 1997). The study also indicates that CK2 could stimulate the DNA binding activity of NRF1 *in vitro*. Because CK2 is an integral component of ncPRC1.3 that inhibits its repressive activity by phosphorylating its RING1A/B component (Gao et al., 2014), CK2 might also promote ncPRC1.3-mediated transcription activation by enhancing NRF1 binding activity *in vivo*, resulting in optimal activation of ncPRC1.3-AUTS2 target genes in the brain.

Evidence involving NRF1 has highlighted its importance in mitochondrial biogenesis (Scarpulla, 2011) and retinal development (Hsiao et al., 2013; Kiyama et al., 2018). Intriguingly, pathways fostering mitochondrial integrity might be critical for those regulating distinct developmental pathways. It is important to emphasize that the reduced volume of the *corpus callosum* observed in *Nrf1* mutant (*Tbr1*$^{CreERT2/+}$*: Nrf1*$^{fx/fx}$*: Pou4f1*$^{CKO/+}$) mice (Figure S6) is a key syndromic feature observed in individuals with RSTS (Cantani and Gagliesi, 1998) as well as in those harboring mutations in the AUTS2 HX repeat domain reported here, strongly supporting that NRF1 and AUTS2 function coordinately in regulating brain development. The *corpus callosum* (CC) connects the cerebral hemispheres and is the largest fiber tract in the brain (Edwards et al., 2014). During development, defects in neurogenesis, telencephalic midline patterning, neuronal migration and specification, axon guidance, and post-guidance development can interrupt CC formation (De León Reyes et al., 2020).

As shown here, ablation of NRF1 or AUTS2 led to defective progenitor-to-MN differentiation *in vitro*. Deletion of NRF1 in the mouse brain and mutations in the AUTS2 HX repeat domain in humans show CC malformation, a common feature of individuals with RSTS (Figure 7). The precise mechanisms by which NRF1 and AUTS2-ncPRC1.3 coordinately regulate gene expression, neuronal differentiation, and, thus, mouse and human brain development and function in postnatal individuals require further investigation. Alternate approaches are needed because deletion of NRF1 or AUTS2 (long and short isoforms) leads to early embryonic lethality. Generation of mouse models carrying mutations in the AUTS2 HX repeat domain might expedite future studies should they recapitulate the RSTS phenotype or other neurological diseases.

Limitations of the study

The data presented here use homozygous mutations/KO cellular models because of the lack of appropriate materials from individuals who exhibit heterozygous mutations in AUTS2. This limitation of our study awaits future determination regarding whether the function of the AUTS2 HX repeat domain is essential for brain development *in vivo*. We generated homozygous knockin mutations in the HX repeat domain of AUTS2 in mESCs, which were then differentiated to MNs to study how the mutations found in affected individuals might affect neurodevelopment. However, the individuals reported in this study harbor heterozygous mutations. Thus, future functional studies based on human induced pluripotent stem cells (iPSCs) or mouse model(s) will provide further conceptual advances toward understanding the etiology of RSTS. Another limitation is that identification of NRF1-mediated AUTS2-ncPRC1.3 recruitment arises from ChIP-seq analyses of AUTS2 and NRF1 in whole-brain extract having assorted cell type specificities. Although NRF1 expression is high in the hippocampus and low in other brain regions (e.g., the cortex), the levels of AUTS2 and PCGF3 are abundant in these NRF1-deficient regions. Thus, our studies are limited to the brain regions having NRF1 expression. Factors other than NRF1 (e.g., USF1/2) likely contribute to AUTS2-ncPRC1.3 recruitment in brain regions deficient in NRF1 expression.

STAR★METHODS

Detailed methods are provided in the online version of this paper and include the following:

- KEY RESOURCES TABLE
- RESOURCE AVAILABILITY
  - Lead contact
  - Materials availability
  - Data and code availability
- EXPERIMENTAL MODEL AND SUBJECT DETAILS
  - Animals
  - Cell lines and culture condition
  - Clinical Cohort
- METHOD DETAILS
  - Immunoprecipitation and Proteomics
  - Whole cell extract and western blotting
  - shRNA-mediated genome editing
  - CRISPR-mediated genome editing
  - Motor Neuron Differentiation
  - Luciferase reporter assay
  - X-gal staining
  - Immuno-histochemical analysis
  - Alkaline phosphatase (AP) staining
  - ChIP-seq library preparation
  - RNA-seq library preparation
  - Single cell RNA-seq library preparation
- QUANTIFICATION AND STATISTICAL ANALYSIS
  - RNA-seq data analysis
  - ChIP-seq data analysis
  - scRNA-seq data analysis

SUPPLEMENTAL INFORMATION

Supplemental information can be found online at https://doi.org/10.1016/j.molcel.2021.09.020.

ACKNOWLEDGMENTS

We thank Drs. Lynne Vales, Esteban Mazzoni, and Anne Schaefer for critical reading of the manuscript as well as past and current Reinberg laboratory members for critical comments and discussions. We also thank the New York University Langone Medical Center (NYULMC) Genome Technology Center for help with sequencing, the NYULMC Cytometry and Cell Sorting Core for help with FACS, and the NYULMC Animal Facility for help with mouse housing. This study utilized computing resources at the High-Performance Computing Facility of the Center for Health Informatics and Bioinformatics at the NYULMC. C.-A.M. and T.K. are supported by grants from the National Institutes of Health-National Eye Institute (EY024376 and P30EY028102). The work in the Reinberg lab is supported by the NIH (R01NS100897 and R01CA199652 to D.R.), the Simon Foundation (240344 to D.R.), and the Howard Hughes Medical Institute.

AUTHOR CONTRIBUTIONS

S.L. and D.R. conceived the project, designed the experiments, and wrote the paper. S.L. performed the vast majority of the experiments and all bioinformatics analyses. K.A.A., C.V.C., M.D., and H.K.M. performed the clinical and genetic analyses under the supervision of W.B.D. W.Z. helped with the luciferase assay. S.G.C., I.I., E.E., C.Z., O.Z., M.S., A.S.P., M.S.P., J.H., M.T.C., A.W., A.S., and L.G. collected the clinical data. T.K. performed the Nrf1 mouse studies under the supervision of T.C.B. and C.-A.M. D.R. supervised the study.

DECLARATION OF INTERESTS

D.R. is a cofounder of Constellation and Fulcrum Pharmaceuticals.

Received: March 29, 2021
Revised: July 21, 2021
Accepted: September 15, 2021
Published: October 11, 2021

REFERENCES

Ajmone, P.F., Avignone, S., Gervasini, C., Giacobbe, A., Monti, F., Costantino, A., Esposito, S., Marchisio, P., Triulzi, F., and Milani, D. (2018). Rubinstein-Taybi syndrome: New neuroradiological and neuropsychiatric insights from a multidisciplinary approach. Am. J. Med. Genet. B. Neuropsychiatr. Genet. *177*, 406–415.

Aldinger, K.A., Timms, A.E., Thomson, Z., Mirzaa, G.M., Bennett, J.T., Rosenberg, A.B., Roco, C.M., Hirano, M., Abidi, F., Haldipur, P., et al. (2019). Redefining the Etiologic Landscape of Cerebellar Malformations. Am. J. Hum. Genet. *105*, 606–615.

Aloia, L., Di Stefano, B., and Di Croce, L. (2013). Polycomb complexes in stem cells and embryonic development. Development *140*, 2525–2534.

Badea, T.C., Cahill, H., Ecker, J., Hattar, S., and Nathans, J. (2009). Distinct roles of transcription factors brn3a and brn3b in controlling the development, morphology, and function of retinal ganglion cells. Neuron *61*, 852–864.

Bannister, A.J., and Kouzarides, T. (1996). The CBP co-activator is a histone acetyltransferase. Nature *384*, 641–643.

Becht, E., McInnes, L., Healy, J., Dutertre, C.-A., Kwok, I.W.H., Ng, L.G., Ginhoux, F., and Newell, E.W. (2018). Dimensionality reduction for visualizing single-cell data using UMAP. Nat. Biotechnol. *37*, 38–44.

Bernstein, B.E., Mikkelsen, T.S., Xie, X., Kamal, M., Huebert, D.J., Cuff, J., Fry, B., Meissner, A., Wernig, M., Plath, K., et al. (2006). A bivalent chromatin structure marks key developmental genes in embryonic stem cells. Cell *125*, 315–326.

Beunders, G., Voorhoeve, E., Golzio, C., Pardo, L.M., Rosenfeld, J.A., Talkowski, M.E., Simonic, I., Lionel, A.C., Vergult, S., Pyatt, R.E., et al. (2013). Exonic deletions in AUTS2 cause a syndromic form of intellectual disability and suggest a critical role for the C terminus. Am. J. Hum. Genet. *92*, 210–220.

Beunders, G., de Munnik, S.A., Van der Aa, N., Ceulemans, B., Voorhoeve, E., Groffen, A.J., Nillesen, W.M., Meijers-Heijboer, E.J., Frank Kooy, R., Yntema, H.G., and Sistermans, E.A. (2015). Two male adults with pathogenic AUTS2 variants, including a two-base pair deletion, further delineate the AUTS2 syndrome. Eur. J. Hum. Genet. *23*, 803–807.

Beunders, G., van de Kamp, J., Vasudevan, P., Morton, J., Smets, K., Kleefstra, T., de Munnik, S.A., Schuurs-Hoeijmakers, J., Ceulemans, B., Zollino, M., et al.; DDD study (2016). A detailed clinical analysis of 13 patients with AUTS2 syndrome further delineates the phenotypic spectrum and underscores the behavioural phenotype. J. Med. Genet. *53*, 523–532.

Bonasio, R., Tu, S., and Reinberg, D. (2010). Molecular signals of epigenetic states. Science *330*, 612–616.

Briggs, J.A., Li, V.C., Lee, S., Woolf, C.J., Klein, A., and Kirschner, M.W. (2017). Mouse embryonic stem cells can differentiate via multiple paths to the same state. eLife *6*, e26945.

Butler, A., Hoffman, P., Smibert, P., Papalexi, E., and Satija, R. (2018). Integrating single-cell transcriptomic data across different conditions, technologies, and species. Nat. Biotechnol. *36*, 411–420.

Cantani, A., and Gagliesi, D. (1998). Rubinstein-Taybi syndrome. Review of 732 cases and analysis of the typical traits. Eur. Rev. Med. Pharmacol. Sci. *2*, 81–87.

Chang, W.-T., Chen, H.I., Chiou, R.-J., Chen, C.-Y., and Huang, A.-M. (2005). A novel function of transcription factor α-Pal/NRF-1: increasing neurite outgrowth. Biochem. Biophys. Res. Commun. *334*, 199–206.

Cohen, I., Zhao, D., Bar, C., Valdes, V.J., Dauber-Decker, K.L., Nguyen, M.B., Nakayama, M., Rendl, M., Bickmore, W.A., Koseki, H., et al. (2018). PRC1 Fine-tunes Gene Repression and Activation to Safeguard Skin Development and Stem Cell Specification. Cell Stem Cell *22*, 726–739.e7.

De León Reyes, N.S., Bragg-Gonzalo, L., and Nieto, M. (2020). Development and plasticity of the corpus callosum. Development *147*, dev189738.

Di Croce, L., and Helin, K. (2013). Transcriptional regulation by Polycomb group proteins. Nat. Struct. Mol. Biol. *20*, 1147–1155.

Dobin, A., Davis, C.A., Schlesinger, F., Drenkow, J., Zaleski, C., Jha, S., Batut, P., Chaisson, M., and Gingeras, T.R. (2013). STAR: ultrafast universal RNA-seq aligner. Bioinformatics *29*, 15–21.

Edwards, T.J., Sherr, E.H., Barkovich, A.J., and Richards, L.J. (2014). Clinical, genetic and imaging findings identify new causes for corpus callosum development syndromes. Brain *137*, 1579–1613.

Elia, J., Gai, X., Xie, H.M., Perin, J.C., Geiger, E., Glessner, J.T., D'arcy, M., deBerardinis, R., Frackelton, E., Kim, C., et al. (2010). Rare structural variants found in attention-deficit hyperactivity disorder are preferentially associated with neurodevelopmental genes. Mol. Psychiatry *15*, 637–646.

Endoh, M., Endo, T.A., Endoh, T., Fujimura, Y., Ohara, O., Toyoda, T., Otte, A.P., Okano, M., Brockdorff, N., Vidal, M., and Koseki, H. (2008). Polycomb group proteins Ring1A/B are functionally linked to the core transcriptional regulatory circuitry to maintain ES cell identity. Development *135*, 1513–1524.

Escobar, T.M., Oksuz, O., Saldaña-Meyer, R., Descostes, N., Bonasio, R., and Reinberg, D. (2019). Active and Repressed Chromatin Domains Exhibit Distinct Nucleosome Segregation during DNA Replication. Cell *179*, 953–963.e11.

Escobar, T.M., Loyola, A., and Reinberg, D. (2021a). Parental nucleosome segregation and the inheritance of cellular identity. Nat. Rev. Genet. *22*, 379–392.

Escobar, T.M., Yu, J.-R., Liu, S., Lucero, K., Vasilyev, N., Nudler, E., and Reinberg, D. (2021b). Inheritance of Repressed Chromatin Domains during S-phase Requires the Histone Chaperone NPM1. bioRxiv. https://doi.org/10.1101/2021.08.31.458436.

Evans, M.J., and Scarpulla, R.C. (1990). NRF-1: a trans-activator of nuclear-encoded respiratory genes in animal cells. Genes Dev. *4*, 1023–1034.

Francis, N.J., Kingston, R.E., and Woodcock, C.L. (2004). Chromatin compaction by a polycomb group protein complex. Science *306*, 1574–1577.

Gao, Z., Zhang, J., Bonasio, R., Strino, F., Sawai, A., Parisi, F., Kluger, Y., and Reinberg, D. (2012). PCGF homologs, CBX proteins, and RYBP define functionally distinct PRC1 family complexes. Mol. Cell *45*, 344–356.

Gao, Z., Lee, P., Stafford, J.M., von Schimmelmann, M., Schaefer, A., and Reinberg, D. (2014). An AUTS2-Polycomb complex activates gene expression in the CNS. Nature *516*, 349–354.

Geng, Z., Wang, Q., Miao, W., Wolf, T., Chavez, J., Giddings, E., Hobbs, R., DeGraff, D.J., Wang, Y., Stafford, J., et al. (2021). AUTS2 controls neuronal lineage choice through a novel PRC1-independent complex and BMP inhibition. bioRxiv. https://doi.org/10.1101/2021.06.29.450402.

Gleyzer, N., Vercauteren, K., and Scarpulla, R.C. (2005). Control of mitochondrial transcription specificity factors (TFB1M and TFB2M) by nuclear respiratory factors (NRF-1 and NRF-2) and PGC-1 family coactivators. Mol. Cell. Biol. *25*, 1354–1366.

Gu, Z., Eils, R., and Schlesner, M. (2016). Complex heatmaps reveal patterns and correlations in multidimensional genomic data. Bioinformatics *32*, 2847–2849.

Guerreiro, R., Brás, J., and Hardy, J. (2015). SnapShot: Genetics of ALS and FTD. Cell *160*, 798–798.e1.

Gugneja, S., and Scarpulla, R.C. (1997). Serine phosphorylation within a concise amino-terminal domain in nuclear respiratory factor 1 enhances DNA binding. J. Biol. Chem. *272*, 18732–18739.

Hagemann-Jensen, M., Ziegenhain, C., Chen, P., Ramsköld, D., Hendriks, G.-J., Larsson, A.J.M., Faridani, O.R., and Sandberg, R. (2020a). Smart-seq3 Protocol. https://www.protocols.io/view/smart-seq3-protocol-7dnhi5e?version_warning=no.

Hagemann-Jensen, M., Ziegenhain, C., Chen, P., Ramsköld, D., Hendriks, G.-J., Larsson, A.J.M., Faridani, O.R., and Sandberg, R. (2020b). Single-cell RNA counting at allele and isoform resolution using Smart-seq3. Nat. Biotechnol. *38*, 708–714.

Hattori, E., Toyota, T., Ishitsuka, Y., Iwayama, Y., Yamada, K., Ujike, H., Morita, Y., Kodama, M., Nakata, K., Minabe, Y., et al. (2009). Preliminary genome-wide association study of bipolar disorder in the Japanese population. Am. J. Med. Genet. B. Neuropsychiatr. Genet. *150B*, 1110–1117.

Hauri, S., Comoglio, F., Seimiya, M., Gerstung, M., Glatter, T., Hansen, K., Aebersold, R., Paro, R., Gstaiger, M., and Beisel, C. (2016). A High-Density Map for Navigating the Human Polycomb Complexome. Cell Rep. *17*, 583–595.

Heinz, S., Benner, C., Spann, N., Bertolino, E., Lin, Y.C., Laslo, P., Cheng, J.X., Murre, C., Singh, H., and Glass, C.K. (2010). Simple combinations of lineage-determining transcription factors prime cis-regulatory elements required for macrophage and B cell identities. Mol. Cell *38*, 576–589.

Hori, K., and Hoshino, M. (2017). Neuronal Migration and AUTS2 Syndrome. Brain Sci. *7*, 54.

Hori, K., Nagai, T., Shan, W., Sakamoto, A., Taya, S., Hashimoto, R., Hayashi, T., Abe, M., Yamazaki, M., Nakao, K., et al. (2014). Cytoskeletal regulation by AUTS2 in neuronal migration and neuritogenesis. Cell Rep. *9*, 2166–2179.

Hsiao, H.-Y., Jukam, D., Johnston, R., and Desplan, C. (2013). The neuronal transcription factor erect wing regulates specification and maintenance of Drosophila R8 photoreceptor subtypes. Dev. Biol. *381*, 482–490.

Huo, L., and Scarpulla, R.C. (2001). Mitochondrial DNA instability and peri-implantation lethality associated with targeted disruption of nuclear respiratory factor 1 in mice. Mol. Cell. Biol. *21*, 644–654.

Jordan, V.K., Fregeau, B., Ge, X., Giordano, J., Wapner, R.J., Balci, T.B., Carter, M.T., Bernat, J.A., Moccia, A.N., Srivastava, A., et al.; Undiagnosed Diseases Network (2018). Genotype-phenotype correlations in individuals with pathogenic RERE variants. Hum. Mutat. *39*, 666–675.

Kapoor, M., Wang, J.-C., Wetherill, L., Le, N., Bertelsen, S., Hinrichs, A.L., Budde, J., Agrawal, A., Bucholz, K., Dick, D., et al. (2013). A meta-analysis of two genome-wide association studies to identify novel loci for maximum number of alcoholic drinks. Hum. Genet. *132*, 1141–1151.

Kasinath, V., Beck, C., Sauer, P., Poepsel, S., Kosmatka, J., Faini, M., Toso, D., Aebersold, R., and Nogales, E. (2021). JARID2 and AEBP2 regulate PRC2 in the presence of H2AK119ub1 and other histone modifications. Science *371*, eabc3393.

Kim, J., and Kingston, R.E. (2020). The CBX family of proteins in transcriptional repression and memory. J. Biosci. *45*, 16.

Kiyama, T., Chen, C.-K., Wang, S.W., Pan, P., Ju, Z., Wang, J., Takada, S., Klein, W.H., and Mao, C.-A. (2018). Essential roles of mitochondrial biogenesis regulator Nrf1 in retinal development and homeostasis. Mol. Neurodegener. *13*, 56.

Kiyama, T., Long, Y., Chen, C.-K., Whitaker, C.M., Shay, A., Wu, H., Badea, T.C., Mohsenin, A., Parker-Thornburg, J., Klein, W.H., et al. (2019). Essential Roles of Tbr1 in the Formation and Maintenance of the Orientation-Selective J-RGCs and a Group of OFF-Sustained RGCs in Mouse. Cell Rep. *27*, 900–915.e5.

Kloet, S.L., Makowski, M.M., Baymaz, H.I., van Voorthuijsen, L., Karemaker, I.D., Santanach, A., Jansen, P.W.T.C., Di Croce, L., and Vermeulen, M. (2016). The dynamic interactome and genomic targets of Polycomb complexes during stem-cell differentiation. Nat. Struct. Mol. Biol. *23*, 682–690.

Korotkevich, G., Sukhov, V., and Sergushichev, A. (2019). Fast gene set enrichment analysis. bioRxiv. https://doi.org/10.1101/060012.

Korsunsky, I., Nathan, A., Millard, N., and Raychaudhuri, S. (2019). Presto scales Wilcoxon and auROC analyses to millions of observations. bioRxiv. https://doi.org/10.1101/653253.

Langmead, B., and Salzberg, S.L. (2012). Fast gapped-read alignment with Bowtie 2. Nat. Methods *9*, 357–359.

Lau, M.S., Schwartz, M.G., Kundu, S., Savol, A.J., Wang, P.I., Marr, S.K., Grau, D.J., Schorderet, P., Sadreyev, R.I., Tabin, C.J., and Kingston, R.E. (2017). Mutation of a nucleosome compaction region disrupts Polycomb-mediated axial patterning. Science *355*, 1081–1084.

LeRoy, G., Oksuz, O., Descostes, N., Aoi, Y., Ganai, R.A., Kara, H.O., Yu, J.-R., Lee, C.-H., Stafford, J., Shilatifard, A., and Reinberg, D. (2019). LEDGF and HDGF2 relieve the nucleosome-induced barrier to transcription in differentiated cells. Sci. Adv. *5*, eaay3068.

Li, H., Handsaker, B., Wysoker, A., Fennell, T., Ruan, J., Homer, N., Marth, G., Abecasis, G., and Durbin, R.; 1000 Genome Project Data Processing Subgroup (2009). The Sequence Alignment/Map format and SAMtools. Bioinformatics *25*, 2078–2079.

Li, G., Margueron, R., Ku, M., Chambon, P., Bernstein, B.E., and Reinberg, D. (2010). Jarid2 and PRC2, partners in regulating gene expression. Genes Dev. *24*, 368–380.

Liao, Y., Smyth, G.K., and Shi, W. (2014). featureCounts: an efficient general purpose program for assigning sequence reads to genomic features. Bioinformatics *30*, 923–930.

Lin, Z., Yang, Z., Xie, R., Ji, Z., Guan, K., and Zhang, M. (2019). Decoding WW domain tandem-mediated target recognitions in tissue growth and cell polarity. eLife *8*, e49439.

Loubiere, V., Papadopoulos, G.L., Szabo, Q., Martinez, A.-M., and Cavalli, G. (2020). Widespread activation of developmental gene expression characterized by PRC1-dependent chromatin looping. Sci. Adv. *6*, eaax4001.

Margueron, R., and Reinberg, D. (2011). The Polycomb complex PRC2 and its mark in life. Nature *469*, 343–349.

Martinez-Delgado, B., Lopez-Martin, E., Lara-Herguedas, J., Monzon, S., Cuesta, I., Juliá, M., Aquino, V., Rodriguez-Martin, C., Damian, A., Gonzalo, I., et al. (2021). De novo small deletion affecting transcription start site of short isoform of AUTS2 gene in a patient with syndromic neurodevelopmental defects. Am. J. Med. Genet. A. *185*, 877–883.

Mazzoni, E.O., Mahony, S., Peljto, M., Patel, T., Thornton, S.R., McCuine, S., Reeder, C., Boyer, L.A., Young, R.A., Gifford, D.K., and Wichterle, H. (2013). Saltatory remodeling of Hox chromatin in response to rostrocaudal patterning signals. Nat. Neurosci. *16*, 1191–1198.

Mefford, H.C., Muhle, H., Ostertag, P., von Spiczak, S., Buysse, K., Baker, C., Franke, A., Malafosse, A., Genton, P., Thomas, P., et al. (2010). Genome-wide copy number variation in epilepsy: novel susceptibility loci in idiopathic generalized and focal epilepsies. PLoS Genet. *6*, e1000962.

Min, J., Zhang, Y., and Xu, R.-M. (2003). Structural basis for specific binding of Polycomb chromodomain to histone H3 methylated at Lys 27. Genes Dev. *17*, 1823–1828.

Narendra, V., Rocha, P.P., An, D., Raviram, R., Skok, J.A., Mazzoni, E.O., and Reinberg, D. (2015). CTCF establishes discrete functional chromatin domains at the Hox clusters during differentiation. Science *347*, 1017–1021.

Ogryzko, V.V., Schiltz, R.L., Russanova, V., Howard, B.H., and Nakatani, Y. (1996). The transcriptional coactivators p300 and CBP are histone acetyltransferases. Cell *87*, 953–959.

Oksenberg, N., and Ahituv, N. (2013). The role of AUTS2 in neurodevelopment and human evolution. Trends Genet. *29*, 600–608.

Oksenberg, N., Haliburton, G.D.E., Eckalbar, W.L., Oren, I., Nishizaki, S., Murphy, K., Pollard, K.S., Birnbaum, R.Y., and Ahituv, N. (2014). Genome-wide distribution of Auts2 binding localizes with active neurodevelopmental genes. Transl. Psychiatry *4*, e431.

Oksuz, O., Narendra, V., Lee, C.-H., Descostes, N., LeRoy, G., Raviram, R., Blumenberg, L., Karch, K., Rocha, P.P., Garcia, B.A., et al. (2018). Capturing the Onset of PRC2-Mediated Repressive Domain Formation. Mol. Cell *70*, 1149–1162.e5.

Orlando, D.A., Chen, M.W., Brown, V.E., Solanki, S., Choi, Y.J., Olson, E.R., Fritz, C.C., Bradner, J.E., and Guenther, M.G. (2014). Quantitative ChIP-Seq normalization reveals global modulation of the epigenome. Cell Rep. *9*, 1163–1170.

Palmer, E.E., Hong, S., Al Zahrani, F., Hashem, M.O., Aleisa, F.A., Ahmed, H.M.J., Kandula, T., Macintosh, R., Minoche, A.E., Puttick, C., et al. (2019). De Novo Variants Disrupting the HX Repeat Motif of ATN1 Cause a Recognizable Non-Progressive Neurocognitive Syndrome. Am. J. Hum. Genet. *104*, 542–552.

Parekh, S., Ziegenhain, C., Vieth, B., Enard, W., and Hellmann, I. (2018). zUMIs - A fast and flexible pipeline to process RNA sequencing data with UMIs. Gigascience *7*, giy059.

Pasini, D., Cloos, P.A.C., Walfridsson, J., Olsson, L., Bukowski, J.-P., Johansen, J.V., Bak, M., Tommerup, N., Rappsilber, J., and Helin, K. (2010). JARID2 regulates binding of the Polycomb repressive complex 2 to target genes in ES cells. Nature *464*, 306–310.

Quinlan, A.R., and Hall, I.M. (2010). BEDTools: a flexible suite of utilities for comparing genomic features. Bioinformatics *26*, 841–842.

Ramírez, F., Ryan, D.P., Grüning, B., Bhardwaj, V., Kilpert, F., Richter, A.S., Heyne, S., Dündar, F., and Manke, T. (2016). deepTools2: a next generation web server for deep-sequencing data analysis. Nucleic Acids Res. *44* (W1), W160-5.

Rose, N.R., King, H.W., Blackledge, N.P., Fursova, N.A., Ember, K.J., Fischer, R., Kessler, B.M., and Klose, R.J. (2016). RYBP stimulates PRC1 to shape chromatin-based communication between Polycomb repressive complexes. Elife *5*, e18591.

Rubinstein, J.H., and Taybi, H. (1963). Broad thumbs and toes and facial abnormalities. A possible mental retardation syndrome. Am. J. Dis. Child. *105*, 588–608.

Scarpulla, R.C. (2011). Metabolic control of mitochondrial biogenesis through the PGC-1 family regulatory network. Biochim. Biophys. Acta *1813*, 1269–1278.

Scelfo, A., Fernández-Pérez, D., Tamburri, S., Zanotti, M., Lavarone, E., Soldi, M., Bonaldi, T., Ferrari, K.J., and Pasini, D. (2019). Functional Landscape of PCGF Proteins Reveals Both RING1A/B-Dependent-and RING1A/B-Independent-Specific Activities. Mol. Cell *74*, 1037–1052.e7.

Schuettengruber, B., Bourbon, H.-M., Di Croce, L., and Cavalli, G. (2017). Genome Regulation by Polycomb and Trithorax: 70 Years and Counting. Cell *171*, 34–57.

Sobreira, N., Schiettecatte, F., Valle, D., and Hamosh, A. (2015). GeneMatcher: a matching tool for connecting investigators with an interest in the same gene. Hum. Mutat. *36*, 928–930.

Stevens, C.A. (1993). Rubinstein-Taybi Syndrome. In GeneReviews, M.P. Adam, H.H. Ardinger, R.A. Pagon, S.E. Wallace, L.J. Bean, K. Stephens, and A. Amemiya, eds. (University of Washington).

Stock, J.K., Giadrossi, S., Casanova, M., Brookes, E., Vidal, M., Koseki, H., Brockdorff, N., Fisher, A.G., and Pombo, A. (2007). Ring1-mediated ubiquitination of H2A restrains poised RNA polymerase II at bivalent genes in mouse ES cells. Nat. Cell Biol. *9*, 1428–1435.

Subramanian, A., Tamayo, P., Mootha, V.K., Mukherjee, S., Ebert, B.L., Gillette, M.A., Paulovich, A., Pomeroy, S.L., Golub, T.R., Lander, E.S., and Mesirov, J.P. (2005). Gene set enrichment analysis: a knowledge-based approach for interpreting genome-wide expression profiles. Proc. Natl. Acad. Sci. USA *102*, 15545–15550.

Sultana, R., Yu, C.-E., Yu, J., Munson, J., Chen, D., Hua, W., Estes, A., Cortes, F., de la Barra, F., Yu, D., et al. (2002). Identification of a novel gene on chromosome 7q11.2 interrupted by a translocation breakpoint in a pair of autistic twins. Genomics *80*, 129–134.

Tavares, L., Dimitrova, E., Oxley, D., Webster, J., Poot, R., Demmers, J., Bezstarosti, K., Taylor, S., Ura, H., Koide, H., et al. (2012). RYBP-PRC1 complexes mediate H2A ubiquitylation at polycomb target sites independently of PRC2 and H3K27me3. Cell *148*, 664–678.

Tong, C.-W., Wang, J.-L., Jiang, M.-S., Hsu, C.-H., Chang, W.-T., and Huang, A.-M. (2013). Novel genes that mediate nuclear respiratory factor 1-regualted neurite outgrowth in neuroblastoma IMR-32 cells. Gene *515*, 62–70.

Trojer, P., and Reinberg, D. (2007). Facultative heterochromatin: is there a distinctive molecular signature? Mol. Cell *28*, 1–13.

Ufartes, R., Berger, H., Till, K., Salinas, G., Sturm, M., Altmüller, J., Nürnberg, P., Thiele, H., Funke, R., Apeshiotis, N., et al. (2020). De novo mutations in FBRSL1 cause a novel recognizable malformation and intellectual disability syndrome. Hum. Genet. *139*, 1363–1379.

Voigt, P., Tee, W.-W., and Reinberg, D. (2013). A double take on bivalent promoters. Genes Dev. *27*, 1318–1338.

Wichterle, H., Lieberam, I., Porter, J.A., and Jessell, T.M. (2002). Directed differentiation of embryonic stem cells into motor neurons. Cell *110*, 385–397.

Wiley, S., Swayne, S., Rubinstein, J.H., Lanphear, N.E., and Stevens, C.A. (2003). Rubinstein-Taybi syndrome medical guidelines. Am. J. Med. Genet. A. *119A*, 101–110.

Yagi, R., Chen, L.-F., Shigesada, K., Murakami, Y., and Ito, Y. (1999). A WW domain-containing yes-associated protein (YAP) is a novel transcriptional co-activator. EMBO J. *18*, 2551–2562.

Yu, G., Wang, L.-G., and He, Q.-Y. (2015). ChIPseeker: an R/Bioconductor package for ChIP peak annotation, comparison and visualization. Bioinformatics *31*, 2382–2383.

Yu, J.-R., Lee, C.-H., Oksuz, O., Stafford, J.M., and Reinberg, D. (2019). PRC2 is high maintenance. Genes Dev. *33*, 903–935.

Zha, X.M., Costa, V., Harding, A.M.S., Reznikov, L., Benson, C.J., and Welsh, M.J. (2009). ASIC2 subunits target acid-sensing ion channels to the synapse via an association with PSD-95. J. Neurosci. *29*, 8438–8446.

Zhang, Y., Liu, T., Meyer, C.A., Eeckhoute, J., Johnson, D.S., Bernstein, B.E., Nusbaum, C., Myers, R.M., Brown, M., Li, W., and Liu, X.S. (2008). Model-based analysis of ChIP-Seq (MACS). Genome Biol. *9*, R137.

Zhou, W., Zhu, P., Wang, J., Pascual, G., Ohgi, K.A., Lozach, J., Glass, C.K., and Rosenfeld, M.G. (2008). Histone H2A monoubiquitination represses transcription by inhibiting RNA polymerase II transcriptional elongation. Mol. Cell *29*, 69–80.

Please cite this article in press as: Liu et al., NRF1 association with AUTS2-Polycomb mediates specific gene activation in the brain, Molecular Cell (2021), https://doi.org/10.1016/j.molcel.2021.09.020

CellPress

STAR★METHODS

KEY RESOURCES TABLE

REAGENT or RESOURCE	SOURCE	IDENTIFIER
Antibodies		
Rabbit anti-AUTS2	Gao et al., 2014	N/A
Rabbit anti-PCGF3	Abcam	Cat# ab201510
Rabbit anti-PCGF5	Abcam	Cat# ab201511
Rabbit anti-Ring1B	Bethyl Laboratories	Cat# A302-869A, RRID:AB_10632773
Rabbit anti-RYBP	Sigma	Cat# PRS2227, RRID:AB_1847589
Rabbit anti-NRF1	Abcam	Cat# ab34682, RRID:AB_2236220
Mouse anti-NRF1	Abcam	Cat# ab55744, RRID:AB_2154534
Mouse anti-P300	Active motif	Cat# 61401, RRID:AB_2716754
Rabbit anti-CBP	Cell Signaling Technology	Cat# 7389, RRID:AB_2616020
Goat anti-Oct4	Santa Cruz Biotechnology	Cat# sc-8628, RRID:AB_653551
Mouse anti-HB9	Developmental Studies Hybridoma Bank	Cat# 81.5C10, RRID:AB_2145209
Rabbit anti-H3	Abcam	Cat# ab1791, RRID:AB_302613
Rabbit anti-H2AK119ub1	Cell Signaling Technology	Cat# 8240; RRID: AB_10891618
Rabbit anti-H3K27me3	Cell Signaling Technology	Cat# 9733; RRID: AB_2616029
Rabbit anti-H3K27ac	Abcam	Cat# ab4729; RRID: AB_2118291
Rabbit anti-H3K4me3	Abcam	Cat# ab8580; RRID: AB_306649
Rabbit anti-Flag	Proteintech	Cat# 20543-1-AP; RRID: AB_11232216
Rabbit anti-Gal4	MilliporeSigma	Cat# 06-262; RRID: AB_310083
Rabbit anti- Cleaved Caspase-3	Cell Signaling Technology	Cat# 9664; RRID: AB_2070042
Rabbit anti-Vinculin	Cell Signaling Technology	Cat# 13901; RRID: AB_2728768
Rabbit anti-GAPDH	Cell Signaling Technology	Cat# 5174; RRID: AB_10622025
Rabbit anti-Drosophila-specific H2Av	Active motif	Cat# 39715, RRID:AB_2793318
Bacterial and virus strains		
Rosetta (DE3) Competent Cells	Novagen	Cat# 70954
One-Shot Stbl3 chemically competent cells	Invitrogen	Cat# C7373-03
DH10Bac	Thermo Fisher Scientific	Cat# 10361012
Chemicals, peptides, and recombinant proteins		
Lipofectamine 2000	Thermo Fisher Scientific	Cat# 11668027
Retinoic Acid	Sigma	Cat# R2625
Smoothened Agonist, SAG	EMD/ Calbiochem	Cat# 566660
Anti-FLAG M2 affinity gel	Sigma	Cat# A2220
FLAG® Peptide	Sigma	Cat# F3290
Leukemia inhibitory factor	Reinberg lab	N/A
CHIR99021	Tocris	Cat# 4423
PD0325901	Sigma	Cat# PZ0162
Dynabeads protein G beads	Thermo Fisher Scientific	Cat# 10003D
SYBR-Gold Nucleic Acid Gel Stain	Thermo Fisher Scientific	Cat# S11494
Agencourt AMPure XP Beads	Beckman Coulter	Cat# A63882
RNase Inhibitor	NEB	Cat# M0314L
Poly Ethylene Glycol (PEG) 8000	Sigma	Cat# 89510-250G-F
GTP	Thermo Fisher Scientific	Cat# R1461
Calcein_AM	Thermo Fisher Scientific	Cat# C1430

(*Continued on next page*)

Please cite this article in press as: Liu et al., NRF1 association with AUTS2-Polycomb mediates specific gene activation in the brain, Molecular Cell (2021), https://doi.org/10.1016/j.molcel.2021.09.020

Continued

REAGENT or RESOURCE	SOURCE	IDENTIFIER
Ethidium homodimer-1	Sigma	Cat# 46043-1MG-F
Tamoxifen	Sigma	Cat #T5648
Critical commercial assays		
Agilent High Sensitivity DNA Kit	Agilent Technologies	Cat# 5067-4626
Nextera XT DNA Library Preparation Kit	illumina	Cat# FC-131-1024
Maxima H Minus Reverse Transcriptase	Thermo Fisher	Cat# EP0751
KAPA HiFi Hotstart PCR kit	Roche	Cat# KK2502
Phusion High-Fidelity DNA Polymerase	NEB	Cat# M0530L
Quant-iT PicoGreen dsDNA Assay Kit	Thermo Fisher	Cat# P7589
RNEasy plus Mini Kit	QIAGEN	Cat# 74134
MinElute PCR Purification Kit	QIAGEN	Cat# 28006
BCA Protein Assay Kit	Thermo Scientific	Cat# 23225
Luciferase Assay System	Promega	Cat# E1500
End-It DNA End-Repair Kit	Lucigen	Cat# ER81050
Klenow Fragment (3′→5′ exo-)	NEB	Cat# M0212L
T4 DNA Ligase (Rapid)	QIAGEN	Cat# 50-305-905
Q5® High-Fidelity DNA Polymerase	NEB	Cat# M0491L
Deposited data		
Deposited raw imaging data	This paper	Mendeley Data: https://doi.org/10.17632/69vsfxr2n6.1
Mouse brain AUTS2, NRF1, RYBP, PCGF3 ChIP-Seq	This study	GEO: GSE161808
E14_ESC AUTS2, NRF1 ChIP-Seq	This study	GEO: GSE161808
Motor neuron AUTS2, NRF1, Ring1B, RYBP, H2AK119ub, H3K27me3, and H3K27ac ChIP-Seq	This study	GEO: GSE161808
Mouse brain, E14_ESC and Motor neuron RNA-Seq	This study	GEO: GSE161808
Motor neuron scRNA-Seq	This study	GEO: GSE161808
Mouse brain input, AUTS2, P300, H2AK119ub, H3K27me3, H3K27ac, H3K4me3, Ring1B and Pol II ChIP-Seq	Gao et al., 2014	GEO: GSE60411
E14_ESC input, Pol II ChIP-Seq	LeRoy et al., 2019	GEO: GSE117155
Motor neuron Pol II, H3K4me3 ChIP-Seq	Narendra et al., 2015	GEO: GSE60240
Experimental models: Cell lines		
Human: HEK293 T-REx	Reinberg lab	N/A
Human: HEK293T 5XGal4TK-Luc	Reinberg lab	N/A
Human: HEK293T 5XGal4TK-Luc GAL4-AUTS2	Reinberg lab	N/A
Human: HEK293T 5XGal4TK-Luc GAL4-AUTS2 P517L	Reinberg lab	N/A
Human: HEK293T 5XGal4TK-Luc GAL4-AUTS2 T534P	Reinberg lab	N/A
Human: HEK293T 5XGal4TK-Luc GAL4-AUTS2 535-542 aa deletion	Reinberg lab	N/A
Human: HEK293T 5XGal4TK-Luc GAL4-AUTS2 sh-PCGF3/5	Reinberg lab	N/A
Mouse: ES cell line E14	Reinberg lab	N/A
Mouse: ES cell line E14 *Auts2* −/−	This study	N/A
Mouse: ES cell line E14 *Nrf1* −/−	This study	N/A
Mouse: ES cell line E14 *Auts2* T534P	This study	N/A
Mouse: ES cell line E14 *Auts2* 535-542 aa deletion	This study	N/A

(*Continued on next page*)

Please cite this article in press as: Liu et al., NRF1 association with AUTS2-Polycomb mediates specific gene activation in the brain, Molecular Cell (2021), https://doi.org/10.1016/j.molcel.2021.09.020

Continued

REAGENT or RESOURCE	SOURCE	IDENTIFIER
Experimental models: Organisms/strains		
Mouse: C57BL/6J	Jackson Laboratory	Strain 000664
Mouse: *Nrf1*-CKO	Kiyama et al., 2018	N/A
Mouse: *Nrf1*-LacZ	Kiyama et al., 2018	N/A
Mouse: *Tbr1*-TauGFP-IRESCreERT2	Kiyama et al., 2019	N/A
Mouse: *Pou4f1*-CKOAP	Badea et al., 2009	Strain 010558
Oligonucleotides		
SgRNA and ssODN for *Auts2*, *Nrf1* knockout, *Auts2* HX mutant knock-in; shRNA targeting human PCGF3/5	This study	See Table S2
Oligonucleotides, Barcode sequence for scRNA-Seq	This study	See Table S3
Recombinant DNA		
pSpCas9(BB)-2A-GFP	Addgene	Cat # 48138
pSpCas9(BB)-2A-GFP-Auts2-KO-sgRNA	This study	N/A
pSpCas9(BB)-2A-GFP-Auts2-T534P-sgRNA	This study	N/A
pSpCas9(BB)-2A-GFP-Auts2-535-542-del-sgRNA	This study	N/A
pSpCas9(BB)-2A-GFP-Nrf1-KO-sgRNA	This study	N/A
PLKO.1 sh-hPCGF3	This study	N/A
PLKO.1 sh-hPCGF5	This study	N/A
pINTO-NFH(empty vector)	Reinberg lab	N/A
pINTO-NFH-AUTS2	This study	N/A
pINTO-NFH-AUTS2-P517L	This study	N/A
pINTO-NFH-AUTS2-T534P	This study	N/A
pINTO-NFH-AUTS2-535-542 del	This study	N/A
pINTO-Gal4(empty vector)	Reinberg lab	N/A
pINTO-Gal4-AUTS2	This study	N/A
pINTO-Gal4-AUTS2- P517L	This study	N/A
pINTO-Gal4-AUTS2-T534P	This study	N/A
pINTO-Gal4-AUTS2-535-542 del	This study	N/A
Software and algorithms		
Bowtie2 v2.4.1	Langmead and Salzberg, 2012	https://github.com/BenLangmead/bowtie2
STAR v2.6.1d	Dobin et al., 2013	https://github.com/alexdobin/STAR
MAC2 v2.1.1	Zhang et al., 2008	https://github.com/macs3-project/MACS
GSEA	Subramanian et al., 2005	https://www.gsea-msigdb.org/gsea/index.jsp
Fgsea	Korotkevich et al., 2019	https://github.com/ctlab/fgsea
BEDTools v2.27.1	Quinlan and Hall, 2010	https://github.com/arq5x/bedtools
Picard v2.18.11	Broad Institute	https://github.com/broadinstitute/picard
HOMER v4.10	Heinz et al., 2010	http://homer.ucsd.edu/
deepTools v3.2.1	Ramírez et al., 2016	https://github.com/deeptools/deepTools
Samtools v1.9	Li et al., 2009	https://github.com/samtools/
ChIPseeker v1.8.6	Yu et al., 2015	https://github.com/YuLab-SMU/ChIPseeker
Integrative Genomics Viewer (IGV)	Broad Institute	https://www.broadinstitute.org/igv/
Prism	GraphPad Software	https://www.graphpad.com/scientific-software/prism/
Benchling	Benchling.com	https://www.benchling.com/
SRA Toolkit	NCBI	https://github.com/ncbi/sra-tools
RStudio	RStudio	httpss://www.rstudio.com/

(*Continued on next page*)

Please cite this article in press as: Liu et al., NRF1 association with AUTS2-Polycomb mediates specific gene activation in the brain, Molecular Cell (2021), https://doi.org/10.1016/j.molcel.2021.09.020

Continued

REAGENT or RESOURCE	SOURCE	IDENTIFIER
R V4.0.0	R-project	https://www.r-project.org/
featureCounts v1.6.3	Liao et al., 2014	https://github.com/torkian/subread-1.6.1
ComplexHeatmap	Gu et al., 2016	https://github.com/jokergoo/ComplexHeatmap
Seurat v3.1.4	Butler et al., 2018	https://github.com/satijalab/seurat
zUMIs v2.9.4	Parekh et al., 2018	https://github.com/sdparekh/zUMIs
Presto	Korsunsky et al., 2019	https://github.com/immunogenomics/presto

RESOURCE AVAILABILITY

Lead contact

Further information and requests for resources and reagents should be directed to and will be fulfilled by the Lead Contact, Danny Reinberg (danny.reinberg@nyumc.org).

Materials availability

All unique/stable reagents generated in this study are available from the Lead Contact with a completed Materials Transfer Agreement.

Data and code availability

- The accession numbers for the raw data FASTQ files and processed files for all sequencing data are deposited in NCBI GEO are GEO: GSE161808. Original gel imaging data can be accessed from Mendeley Data: DOI: https://doi.org/10.17632/69vsfxr2n6.1.
- This paper does not report original code.
- Any additional information required to reanalyze the data reported in this paper is available from the lead contact upon request.

EXPERIMENTAL MODEL AND SUBJECT DETAILS

Animals

We did not observe any sex/gender influence on results derived from mice or patients. All mice were housed with a 12 hour light-dark cycle. Mixed cohorts of female and male mice were used for all experiments to minimize gender effects. Mice used for ChIP-Seq and biochemical assays were from various developmental stages as indicated in Figure legend. Mice used for Tamoxifen injection to delete NRF1 were 2 to 3 months old. All animal procedures followed the US Public Health Service Policy on Humane Care and Use of Laboratory Animals and were approved by the Animal Welfare Committee at New York University and the University of Texas McGovern Medical School at Houston.

Cell lines and culture condition

All ESC lines (E14 and derivatives) were grown in DMEM supplemented with 15% FBS, L-glutamine, penicillin/streptomycin, sodium pyruvate, non-essential amino acids, 0.1 mM β-mercaptoethanol, LIF, and 2i inhibitors, which include 1 μM MEK1/2 inhibitor (PD0325901) and 3 μM GSK3 inhibitor (CHIR99021) on 0.1% gelatin coated plates.

HEK293 T-Rex and HEK293T 5XGal4TK-Luc cells were cultured in standard DMEM supplemented with 10% FBS, 100 U/mL penicillin-streptomycin.

WT and mutant NFH-AUTS2 inducible cell lines were obtained by transfecting each pINTO-NFH plasmid into 293 T-Rex cells, and WT and mutant Gal4-AUTS2 inducible cell lines were obtained by transfecting each pINTO-Gal4 plasmid into HEK293T 5XGal4TK-Luc cells. Transfected cells were seeded at limiting dilutions, and isolated clones were screened by western blot.

Clinical Cohort

The initial proband (LR05-007) was identified through trio-based exome sequencing in a cohort of 100 individuals with cerebellar malformations (Aldinger et al., 2019). We recruited 6 additional individuals with *de novo* pathogenic or likely pathogenic variants in *AUTS2* by sharing data through GeneMatcher (Sobreira et al., 2015) or through collaboration with colleagues. The 7 individuals in this cohort (2 females, 5 males) were 1 to 15.5 years of age at the time of their most recent evaluation. We obtained clinical data for all patients, including features tabulated in a reported AUTS2 clinical severity score (Beunders et al., 2013, 2015, 2016). Written informed consent was obtained from all participants through protocols approved by Institutional Review Boards at the local institution or at Seattle Children's Hospital.

Please cite this article in press as: Liu et al., NRF1 association with AUTS2-Polycomb mediates specific gene activation in the brain, Molecular Cell (2021), https://doi.org/10.1016/j.molcel.2021.09.020

CellPress

METHOD DETAILS

Immunoprecipitation and Proteomics

Cell pellets were prepared from cell culture plates or mouse brain. Nuclei were extracted using HMSD buffer (20 mM HEPES, pH 7.5 at 4°C, 5 mM $MgCl_2$, 250 mM sucrose, 25 mM NaCl, 1 mM DTT) supplemented with protease inhibitors (0.2 mM PMSF, 1 μg/mL Pepstatin A, 1 μg/mL Leupeptin, and 1 μg/mL Aprotinin) and phosphatase inhibitors (10 mM NaF and 1 mM Na_3VO_4), and incubated on ice for 5 min. Lysates were pelleted at 3,000 rpm for 5 min at 4°C and nuclei pellets were washed one more time with HMSD buffer. The resulting nuclei pellets were resuspended in BC420 high salt buffer (20 mM Tris-HCl at pH 7.9, 1.5 mM $MgCl_2$, 0.42 M NaCl, 0.5 mM DTT, 0.2 mM EDTA) supplemented with protease inhibitors and phosphatase inhibitors for lysing at 4°C for 1 hr with occasional pipetting. Lysates were then pelleted at 20,000 x g for 15 min at 4°C. Finally, supernatants were collected and subjected to dialysis in Buffer D (20 mM HEPES, 150 mM NaCl, 1.5 mM $MgCl_2$, 0.2 mM EDTA, and 5% glycerol) overnight at 4°C. Prior to any subsequent applications, nuclear extracts were centrifuged again at 20,000 g for 10 min at 4°C to remove any precipitate. Supernatants were collected, and protein concentrations were quantified via bicinchonic acid (BCA) assay. For immunoprecipitation, 1-2 mg of nuclear extract was incubated with 1∼3 μg of antibody. After incubation at 4°C for 2 hr, 30 ul of protein G beads were added for incubation at 4°C overnight. Beads were washed three times with Buffer D (20 mM HEPES, 150 mM NaCl, 1.5 mM $MgCl_2$, 0.2 mM EDTA, and 5% glycerol), and eluted with 0.2 M glycine (pH 2.6) or 1 × SDS loading buffer. Proteins from immunoprecipitation were separated by SDS–PAGE, using 4%–12% NuPAGE Novex Bis–Tris gels and then stained with Coomassie Blue. Bands were excised from gels and digested with trypsin, followed by standard LC-MS/MS procedure.

Whole cell extract and western blotting

Cells were harvested and lysed with CHAPS-Urea buffer (50 mM Tris-HCl, pH 7.9, 8M Urea, and 1% CHAPS) containing protease inhibitors and phosphatase inhibitors as mentioned above. The cell suspension was briefly sonicated (40% amplitude, 5 strokes) and centrifuged at 20,000 x g at 4°C for 20 min. The supernatant was collected and protein concentrations were quantified via bicinchonic acid (BCA) assay. Proteins were separated using a 6%–12% SDS-PAGE gel, and transferred onto a PVDF membrane. Membranes were blocked with 5% milk in PBST at RT for 1 hr and incubated with primary antibody overnight at 4°C. Membranes were washed 3 times with PBST and then incubated with HRP-conjugated secondary antibodies for 1 hr at RT, followed by exposure.

shRNA-mediated genome editing

Oligos designed for knockdown (see Table S2) were annealed and cloned into PLKO.1-shRNA vector using Age1 and EcoR1 restriction sites. The resulting plasmids were transfected into 293TRex cells using Neon Transfection System with parameter: 1500V, 1 pulse of 30ms. The cells were subject to puromycin selection at 1 ug/ml for 4 days. The efficiency of knockdown was confirmed by western blot.

CRISPR-mediated genome editing

To generate stable *Auts2* and *Nrf1* KO cell lines, sgRNAs were designed using CRISPR design tool in https://benchling.com/faq. sgRNAs in Table S1 were cloned in pSpCas9(BB)-2A-GFP (PX458, a gift from Feng Zhang, Addgene plasmid #48138) and transfected into mESCs, using Lipofectamine 2000 (Life Technologies). GFP-positive cells were sorted 48 hr after transfection and 20,000 cells were plated on a 15 cm dish. Single mESC was allowed to grow to a colony for ∼5 days and then was picked, trypsinized in Accutase for 5 min, and split into two individual wells of two 96-well plates for genotyping and culture, respectively. Genomic DNA was extracted using lysis buffer (50 mM Tris-HCl, pH 8, 2 mM NaCl, 10 mM EDTA, 0.1% SDS) supplemented with protease K, and genotyping PCRs were performed using primers (Table S2) surrounding the target site. The resulting PCR products were sent for sequencing to determine the presence of a deletion or a mutation event. Clones were further confirmed by western blot.

For endogenously knock-in the mutations in AUTS2 HX repeat in mESC, a ssODN donor used for homology directed repair and CRISPR/Cas9 plasmid (px458) with designed sgRNA (see Table S2 also) were co-transfected into mESCs, using Lipofectamine 2000. The following FACS, colony picking and characterization are the same as generating KO lines described above.

Motor Neuron Differentiation

E14 mouse embryonic stem cells (mESCs) were cultured in standard medium supplemented with LIF, and 2i conditions as described above. For motor neuron (MN) differentiation, the previously described protocol was applied (Narendra et al., 2015). Briefly, about 4 million mESCs were plated in a 500 cm^2 square dish and differentiated into embryoid bodies in AK medium (250 mL advanced DMEM/F12, 250 mL neurobasal medium, 75 mL knockout serum, L-glutamine, penicillin/streptomycin, 0.1 mM β-mercaptoethanol) for 2 days. Embryoid bodies were then diluted by 1:4 and further patterning was induced by freshly adding 1 μM all-trans-retinoic acid (RA) and 0.5 μM smoothened agonist (SAG) for an additional 4 days. Fresh medium was added after 2 days to support motor neuron survival.

Luciferase reporter assay

HEK293T 5XGal4 TK-Luc cells stably transfected with pINTO-GAL4 vector control or with inserts of interest were treated with 100 ng/ml doxycycline. Cells were lysed by adding 250 ul of ice-cold lysis buffer (0.2% Triton X-100, 100 mM potassium phosphate, pH 7.8,

Please cite this article in press as: Liu et al., NRF1 association with AUTS2-Polycomb mediates specific gene activation in the brain, Molecular Cell (2021), https://doi.org/10.1016/j.molcel.2021.09.020

and 1 mM DTT) and shaking for 10 min at 4°C. The cell lysate was centrifuged at 20,000 g for 10 min and the protein concentration of the resulting supernatant was determined by bradford Assay. 30 ug of the supernatant was assayed for luciferase activity using luciferase assay substrate (Promega).

X-gal staining

Mouse brain was fixed by perfusion with 10% neutral buffered formalin. Extracted brain was embedded in OCT compound then sectioned into 50 um thickness. Sections were dried at RT for 3 hr and then washed with wash buffer (0.1 M sodium phosphate containing 2 mM $MgCl_2$, 0.01% deoxycholate, and 0.02% Nonidet P-40, pH 7.3). LacZ color reaction was performed in wash buffer containing 5 mM potassium ferrocyanide, 5 mM potassium ferricyanide, and 1 mg/ml X-gal at 37°C overnight. Color reaction was terminated by incubation in 10% formalin for 10 min. Post-fixed sections were washed, dehydrated, and mounted with Cytoseal 60 (Thermo Fisher Scientific). Images were collected with a Canon EOS 10 digital camera (Melville, NY) mounted on an Olympus IX71 microscope.

Immuno-histochemical analysis

Mouse brain was fixed by perfusion with 10% neutral buffered formalin. Extracted brain was embedded in OCT compound, and then sectioned into 100 um thickness. Sections were incubated with anti-GFP (1:1000, Invitrogen) antibody. Alexa 488 conjugated secondary antibody was used in 1:800 dilution (Jackson Immuno-reserach).

Alkaline phosphatase (AP) staining

Tbr1$^{CreERT2/+}$*:Nrf1*$^{fx/+}$*:Pou4f1*$^{CKO/+}$ and *Tbr1*$^{CreERT2/+}$*:Nrf1*$^{fx/fx}$*:Pou4f1*$^{CKO/+}$ mice (2 to 3 months old) were intraperitoneally injected with tamoxifen (5 consecutive daily injections of 100 ug/g body weight), and then used for AP staining 3 months after tamoxifen injection. Brains were fixed by perfusion with 10% neutral buffered formalin. Fixed brain was embedded in OCT compound and sectioned into 100 um thickness. Retinal flat-mounts were fixed in 10% neutral buffered formalin for 10 min at RT. Brain sections and retinas were incubated in heated PBS for 30 min in a 65°C water bath to inactivate endogenous AP activity. AP color reaction was performed in 0.1 M Tris, pH 9.5, 0.1 M NaCl, 50 mM $MgCl_2$, 0.34 g/ml nitroblue tetrazolium and 0.175 g/ml 5-bromo-4-chrolo-3-indolyl-phosphate for overnight at RT. Stained tissues were washed three times in PBS, post-fixed with 10% neutral buffered formalin, dehydrated with a series of ethanol, then cleared with 2:1 benzyl benzoate/benzyl alcohol. Tiled images were collected using a Zeiss Axio Imager 2 microscope (Carl Zeiss).

ChIP-seq library preparation

For cross-linking, ESCs were fixed in 1% formaldehyde for 10 min at RT directly on plates and quenched with 125 mM glycine for 5 min at RT. For cross-linking of MN, ESC-derived motor neuron cultured for 6 days were dissociated with 0.05% trypsin, neutralized, fixed in 1% formaldehyde for 15 min at RT and then quenched with 125 mM glycine for 5 min at RT. For cross-linking of mouse brain, mouse whole brains were quickly dissected at postnatal day one and homogenized with a glass douncing homogenizer using first a loose, then a tight pestle. The cell homogenate was fixed with a final concentration of 1% formaldehyde for 10 min at RT and the reaction was quenched with 0.125 M glycine for 5 min at RT.

Cell pellets were washed twice in PBS and nuclei were isolated using buffers in the following order: LB1 (50 mM HEPES, pH 7.5 at 4°C, 140 mM NaCl, 1 mM EDTA, 10% Glycerol, 0.5% NP40, 0.25% Triton X; 10 min at 4°C), LB2 (10 mM Tris, pH 8 at 4°C, 200 mM NaCl, 1 mM EDTA, 0.5 mM EGTA; 10 min at 4°C), and LB3 (10 mM Tris, pH 7.5 at 4°C, 1 mM EDTA, 0.5 mM EGTA, and 0.5% N-Lauroylsarcosine sodium salt). Chromatin was fragmented to an average size of 250 bp in LB3 buffer using a Diagenode Bioruptor. 200 μg sonicated chromatin, 4 ug antibody and 20 ul Dynabeads were used in each ChIP reaction supplemented with 0.5x volumn of incubation buffer (3% Triton X, 0.3% Na Deoxycholate, 15 mM EDTA). 1 μg of *Drosophila* chromatin and 0.2 μg of anti-*Drosophila* H2A.X antibody were added in each ChIP reaction as spike-in references, except 3 μg of *Drosophila* chromatin was used for H3K27ac and H2AK119ub ChIP. After 5 consecutive washes with RIPA buffer (50 mM HEPES, pH 7.5 at 4°C, 0.7% Na Deoxycholate, 1 mM EDTA, 1% NP40, 500 mM LiCl) and one wash with TE+50 mM NaCl, the beads-bound DNA was eluted in freshly prepared elution buffer (50 mM Tris, pH 8, 10 mM EDTA, 1% SDS) at 65°C for 20 min. Eluted DNA was de-crosslinked at 65°C overnight, followed by protease K and RNase A treatment.

For Library preparation, IP'ed DNA (~1-30 ng) was end-repaired using End-It Repair Kit, tailed with deoxyadenine using Klenow exo-, and ligated to custom adapters with T4 Rapid DNA Ligase (Enzymatics). Fragments of 200-600 bp were size-selected using Agencourt AMPure XP beads (0.5X and 0.3X), and subjected to PCR amplification using Q5 DNA polymerase. Libraries were size-selected using Agencourt AMPure XP beads (0.75X), quantified by Qubit dsDNA HS Assay Kit and quality checked by High Sensitivity D1000 ScreenTape. Libraries were sequenced as 50 bp single-end reads on the Illumina HiSeq 4000 platform.

RNA-seq library preparation

Total RNA was isolated with Tripure isolation reagent and gDNA was removed by RNeasy Plus mini kit. PolyA+ RNA was isolated from 5 ug total RNA using Dynabeads Oligo$(dT)_{25}$, fragmented with Mg^{2+} contained in the 1st strand buffer at 94°C for 15 min, and reverse transcribed using Superscript III and random hexamers to synthesize the first strand cDNA. Single strand cDNA was precipitated and dTTP was removed by phenol/chloroform/isoamyl alcohol extraction and ethanol precipitation. Second strand cDNA was

Please cite this article in press as: Liu et al., NRF1 association with AUTS2-Polycomb mediates specific gene activation in the brain, Molecular Cell (2021), https://doi.org/10.1016/j.molcel.2021.09.020

synthesized with dUTP to generate strand asymmetry using DNA Pol I and *E. coli* ligase, and then purified by MinElute PCR Purification Kit. Double-stranded DNA was end-repaired, A-tailed, and ligated to custom barcode adapters as described above. RNA-seq libraries were sequenced as 50 bp paired-end reads on the Illumina HiSeq 4000 platform or NovaSeq 6000 platform.

Single cell RNA-seq library preparation

For single cell RNA-seq library preparation, we chose the newly developed Smart-seq3 technique (Hagemann-Jensen et al., 2020a, 2020b), an improved version of Smart-seq2 with a 5′-unique molecular identifier RNA counting strategy and a much higher sensitivity that detects thousands more transcripts per cell. The library was generated according to the published protocol (Hagemann-Jensen et al., 2020a, 2020b), with the following modifications. ESC-derived motor neuron cultured for 6 days were dissociated with 0.05% trypsin and stained with 0.2 uM Calcein AM and 8 uM Ethidium homodimer-1 at RT for 15 min. Single viable cells were sorted using Fluorescence Activated Cell Sorting to single wells of 96-well fully-skirted Eppendorf PCR plates in 3 uL lysis buffer (5% PEG8000, 0.1% Triton X-100, 0.5 unit/ul RNase Inhibitor, 0.5 uM OligodT_{30}VN, 0.5 mM dNTP in nuclease free water). The plates were immediately covered, spun at 2000 rpm for 1 min at 4°C, and stored at −80°C until further analysis. In each plate, well A1 was left empty and 100 cells were sorted to well H1 for quality control and they were excluded for downstream analysis.

Plates were incubated at 72°C for 10 min for lysing the cells and denaturing the RNA. Next, 1 μl of reverse transcription mix (25 mM Tris-HCl, pH 8, 30 mM NaCl, 1 mM GTP, 2.5 mM $MgCl_2$, 8 mM DTT, 0.5 unit/ul RNase Inhibitor, 2 μM Smart-seq3 TSO, 2 unit/ul Maxima H-minus reverse transcriptase enzyme) was added to each well for reverse transcription and template switching at 42°C for 90 min followed by 10 cycles at 50°C for 2 min and at 42°C for 2 min and the reaction was inactivated at 85°C for 5 min. cDNA pre-amplification was performed by adding 6 μl of PCR mix (1 × Kapa HiFi HotStart buffer, 0.02 unit/ul KAPA HiFi DNA polymerase, 0.5 mM $MgCl_2$, 0.3 mM dNTPs, 0.5 μM Smartseq3 forward PCR primer and 0.1 μM Smartseq3 reverse PCR primer) with the following protocol: 3 min at 98°C for initial denaturation, 18–24 cycles of 20 s at 98°C, 30 s at 65°C and 6 min at 72°C, followed by a final elongation for 5 min at 72°C. PCR cycles were determined for each cell type by prior experiments and 19 cycles were used for motor neuron to obtain ∼10 ng purified cDNA.

Pre-amplified cDNA was purified by 0.6x volume of AMpure XP beads, eluted in 14 ul nuclease free water, quantified using the Quant-iT PicoGreen dsDNA Assay Kit and size distributions were checked on a high-sensitivity DNA chip. cDNA was then diluted to 200 pg/μl, and 1 ul was used for tagmentation by mixing with 1 μl of tagmentation reaction mixture (10 mM TAPS, pH 8.5, 5 mM $MgCl_2$, 8% PEG8000, 0.08 ul Tn5 mix (illumina)). The reaction was performed at 55°C for 7 min, followed by heat inactivation at 80°C for 5 min. Library amplification of the tagmented samples was performed using custom-designed index primers and by adding 5 μl of PCR mix (1 × Phusion High-Fidelity buffer, 0.01 unit/ul Phusion High-Fidelity DNA Polymerase, 0.2 mM dNTPs, 0.1 μM forward indexed primer and 0.1 μM reverse indexed primer). Amplification was performed as follows: 3 min 72°C; 30 s at 95°C; 12 cycles of (10 s at 95°C; 30 s at 55°C; 30 s at 72°C); and 5 min at 72°C. Samples from one 96-well plate were pooled, and then purified with 0.6x volume of Ampure XP beads. Libraries were quantified by Qubit dsDNA HS Assay Kit and quality checked on a high-sensitivity DNA chip. The size averaged at ∼1 Kb should be expected. scRNA-seq libraries were sequenced as 50 bp paired-end reads on the Illumina NovaSeq 6000 platform and importantly, ∼20% phiX spike-in was added to resolve the low complexity issue in the first 20 bps. All oligos used are listed in Table S3.

QUANTIFICATION AND STATISTICAL ANALYSIS

RNA-seq data analysis

Reads were aligned to the mouse reference genome mm10 using STAR with parameters:–outFilterMismatchNoverLmax 0.2–outFilterMultimapNmax 1–outSAMstrandField intronMotif–outSAMmapqUnique 60–twopassMode Basic–outSJfilterReads Unique–outFilterIntronMotifs RemoveNoncanonical. Gene counts were calculated using featureCounts with parameters: -p -s 2 -t exon, and RefSeq mm10 annotation downloaded from GENCODE. The output gene count tables were used as input into DeSeq2 for normalization and differential expression analysis. For comparing the expression level of different genes within a sample, TPM (transcripts per kilobase million) is calculated as: TPM = (CDS read count * mean read length * 10^6) / (CDS length * total transcript count)

ChIP-seq data analysis

Reads were aligned to the mouse reference genome mm10 and dm6 for spike-in samples, using Bowtie2 with default parameters. Reads of quality score less than 30 were removed using samtools and PCR duplicates were removed using picard. Regions in mm10 genome blacklist was removed using bedtools and bigwig files were generated using deeptools and parameters:–binSize 50–normalizeUsing RPKM–ignoreDuplicates–ignoreForNormalization chrX–extendReads 250 for visualization in IGV. Peaks were called using MACS2 with parameters: -g mm–keep-dup 1–nomodel–extsize 300. Genomic peak annotation was performed with the R package ChIPseeker considering the region ± 3 kb around the TSS as the promoter. Peak overlapping analysis was performed using the Python package Intervene and visualized using the Python package Matplotlib. Motif discovery was performed using narrowPeak files generated by MACS2 and findMotifsGenome.pl function from HOMER with default parameters: mm10 -size given -mask –preparse.

Please cite this article in press as: Liu et al., NRF1 association with AUTS2-Polycomb mediates specific gene activation in the brain, Molecular Cell (2021), https://doi.org/10.1016/j.molcel.2021.09.020

For visualization of ChIP-seq, uniquely aligned reads mapping to the mouse genome were normalized using dm6 spike-in as described previously (Orlando et al., 2014). Heatmaps were performed using the functions computeMatrix followed by plotHeatmap and plotProfile from deepTools. All ChIP-Seq files presented in Figures 5C and 5H were used as input to computeMatrix and plotHeatmap for K-means clustering. Violin plots for ChIP-Seq signal were prepared by multiBigwigSummary in BED-file mode from deepTools using as bed file the regions corresponding to Ring1B cluster 3 regions. The resulting tab-delimited raw-count file was used as input to ggplot2 for Violin plot.

scRNA-seq data analysis

Raw non-demultiplexed fastq files were processed using zUMIs with STAR to generate expression profiles for both the 5′ ends containing UMIs as well as combined full-length and UMI data. The parameters: find pattern: ATTGCGCAATG, UMI (12-19), cDNA (23-50) were specified for Read 1. The UMI count table containing both intron and exon reads was used by Seurat for downstream analysis. Cells with more than 3000 genes detected and less than 5% of reads mapping to mitochondrial genome were retained. Data were normalized (scTransform) and used for principal component analysis dimensionality reduction, followed by louvain clustering and UMAP dimensionality reduction. Major cell types were readily identifiable by common marker genes: posterior neural progenitor (PNP) expressing Sox3, posterior and ventral neural progenitor (PVNP) expressing Hoxd4, newborn motor neuron (NMN) expressing Neurog2, and motor neuron (MN) expressing Mnx1 and Chat. The percentage of each cell type from each sample was used as input to ggplot2 for stack area plot.

Differential gene expression analysis between defined cell clusters was performed using R package presto. The top 500 DEGs were ordered by p value. Averaged expression among the defined cell clusters was scaled by row and used as input to R package ComplexHeatmap for visualization. Regions of AUTS2-PRC1 and NRF1 co-localization were identified using peak files generated by MACS2 and bedtools intersect function with default parameters. Co-targeted genes with its promoter located in the overlapped regions were identified by R package ChIPseeker with default parameters. The normalized expression of those genes in MN population was calculated using R package presto and used as input to ggplot2 for scatterplot.